Original Article

A novel cuproptosis-related lncRNA signature to predict prognosis and immune landscape of lung adenocarcinoma

Xinyi Wang^, Hui Jing, Hecheng Li^

Department of Thoracic Surgery, Ruijin Hospital, Shanghai Jiao Tong University School of Medicine, Shanghai, China

Contributions: (I) Conception and design: All authors; (II) Administrative support: H Li; (III) Provision of study materials or patients: X Wang, H Jing; (IV) Collection and assembly of data: X Wang, H Jing; (V) Data analysis and interpretation: X Wang; (VI) Manuscript writing: All authors; (VII) Final approval of manuscript: All authors.

Correspondence to: Hecheng Li; Hui Jing. Department of Thoracic Surgery, Ruijin Hospital, Shanghai Jiao Tong University School of Medicine, 197 Ruijin 2nd Road, Shanghai 200025, China. Email: lihecheng2000@hotmail.com; qyjinghui@163.com.

Background: Cuproptosis, a recently discovered type of programmed cell death (PCD), paves a new avenue for cancer treatment. It has been revealed that PCD-related lncRNAs play a critical role in various biological processes of lung adenocarcinoma (LUAD). However, the role of cuproptosis-related lncRNA (CuRLs) remains unclear. This study aimed to identify and validate a CuRLs-based signature for the prognostic prediction of patients with LUAD.

Methods: RNA sequencing data and clinical information of LUAD were obtained from The Cancer Genome Atlas (TCGA) and Gene Expression Omnibus (GEO) databases. Pearson correlation analysis was used to identify CuRLs. Univariate Cox regression analysis, Least Absolute Shrinkage and Selection Operator (LASSO) Cox regression, and stepwise multivariate Cox analysis were applied to construct a novel prognostic CuRLs signature. A nomogram was developed for the prediction of patient survival outcomes. Gene set variation analysis (GSVA), gene set enrichment analysis (GSEA), Gene Ontology (GO), and Kyoto Encyclopedia of Genes and Genomes (KEGG) pathway analyses were utilized to explore potential functions underlying the CuRLs signature. Patients were divided into low- and high-risk groups. Several algorithms, such as tumor immune estimation resource (TIMER), cell-type identification by estimating relative subsets of RNA transcripts (CIBERSORT), and QuanTIseq, were combined to comprehensively investigate the differences in immune landscape between different risk groups. Sensitivity to common anticancer drugs was analyzed using the pRRophetic algorithm.

Results: We constructed a novel prognostic signature based on 10 CuRLs, including *CARD8-AS1*, *RUNDC3A-AS1*, *TMPO-AS1*, *MIR31HG*, *SEPSECS-AS1*, *DLGAP1-AS1*, *LINC01137*, *ZSCAN16-AS1*, *APTR*, and *ELOA-AS1*. This 10-CuRLs risk signature showed great diagnostic accuracy combined with traditional clinical risk factors, and a nomogram was constructed for potential clinical translation. The tumor immune microenvironment was significantly different between different risk groups. Among drugs commonly used in the treatment of lung cancer, the sensitivity of cisplatin, docetaxel, gemcitabine, gefitinib, and paclitaxel was higher in low-risk patients, and patients in the low-risk group may benefit more from imatinib.

Conclusions: These results revealed the outstanding contribution of the CuRLs signature to the evaluation of prognosis and treatment modalities for patients with LUAD. The differences in characteristics between different risk groups provide an opportunity for better patient stratification and to explore novel drugs in different risk groups.

Keywords: Lung adenocarcinoma; cuproptosis; lncRNA; prognostic prediction; immune landscape

^ ORCID: Xinyi Wang, 0000-0002-6926-5934; Hecheng Li, 0000-0001-8069-6033.

Submitted Jul 02, 2022. Accepted for publication Jan 02, 2023. Published online Feb 23, 2023.
doi: 10.21037/tlcr-22-500
View this article at: https://dx.doi.org/10.21037/tlcr-22-500

Introduction

Lung cancer accounts for the highest cancer-related mortality rate worldwide, of which lung adenocarcinoma (LUAD) is the most common subtype (1). For all stages of lung cancer combined, the 5-year survival rate is around 22%. Despite progress made in the fields of surgery, chemotherapy, radiotherapy, and immunotherapy, there is still much room for improvement in cancer treatment. Thus, novel molecular biomarkers provide additional prognostic value and better risk assessment to guide personalized therapy.

The existence and physiological significance of programmed cell death (PCD) have garnered increasing interest in recent years, including necroptosis, apoptosis, pyroptosis, and ferroptosis (2,3). PCD has shown great potential in cancer treatment, and the induction of cell deaths combined with immune checkpoint inhibitors (ICIs) has shown synergistically enhanced antitumor efficacy (3). Copper-induced cell death, termed cuproptosis, is recently recognized as a new form of PCD (4). Unlike other types of cell death, cuproptosis occurs through the direct binding of copper to lipoylated components of the tricarboxylic acid cycle, leading to the aggregation of lipoylated protein and the subsequent loss of iron-sulfur cluster protein, finally causing proteotoxic stress and cell death. Copper, a redox-active metal ion, is essential for most animals. It serves as a catalytic and structural cofactor for enzymes and plays a vital role in oxygen transport, cellular metabolism, energy generation, and signal transduction (5). Copper concentrations are maintained at a low level under normal physiological conditions by a homeostatic mechanism (6). Abnormal accumulation of copper is frequently observed in several cancers, leading to tumor proliferation, angiogenesis, and metastasis (7,8). SLC3A1, known as CTR1, is a transmembrane copper transporter protein. Research showed that SLC3A1-dependent copper level was associated with the malignant degree of pancreatic cancer (9). In addition, the combination of copper and copper ionophore disulfide has been found to enhance the sensitivity of patients with head and neck squamous cell carcinoma to cisplatin (10). Therefore, the underlying mechanism of cuproptosis discovered by Tsvetkov *et al.* presents novel avenues for applying cuproptosis in cancer treatment (4). Considering the great potential of cuproptosis in cancer treatment, cuproptosis-related genes are promised to be novel therapeutic targets. The investigation of molecular characteristics of cuproptosis in cancer patients may provide new prognostic and therapeutic methods.

Long non-coding RNAs (lncRNAs) are non-coding RNA transcripts longer than 200 nucleotides (11). Numerous studies have noted that lncRNAs participate in various biological processes of LUAD (12-14). For example, the novel lncRNA lung cancer associated transcript 3 (LCAT3) promoted proliferation and metastasis of lung cancer cells via the recruitment of far upstream element binding protein 1 (FUBP1) to activate c-MYC (13). Recently, there has been a surge of interest in the relationship between lncRNAs and PCD (15). Various studies have shown that PCD-related lncRNAs could be used as prognostic markers to predict the response to immunotherapy and patient outcomes (16-18). Thus, the identification of cuproptosis-related lncRNAs (CuRLs) is significant for elucidating the molecular mechanism of LUAD and helping us realize the potential of cuproptosis in cancer treatment.

The present study identified CuRLs from The Cancer Genome Atlas (TCGA) dataset and constructed a risk signature based on 10 prognostic CuRLs. We developed and validated a nomogram for clinical use that integrated the 10-CuRLs signature and clinical factors. The applicability of this risk signature was validated in the Gene Expression Omnibus (GEO) meta-cohort. In addition, gene set variation analysis (GSVA), gene set enrichment analysis (GSEA), Gene Ontology (GO), and Kyoto Encyclopedia of Genes and Genomes (KEGG) analysis were performed to explore the underlying biological mechanisms of the 10-CuRLs signature comprehensively. Then, the differences between low- and high-risk groups were compared in immune infiltration, tumor mutation burden (TMB), and drug response, shedding light on the potential role of CuRLs in cancer treatment. We present the following article in accordance with the TRIPOD reporting checklist (available at https://tlcr.amegroups.com/article/view/10.21037/tlcr-22-500/rc).

Methods

Data acquisition

RNA sequencing data and clinical information for LUAD were obtained from TCGA (https://cancergenome.nih.gov/) database, which included 526 tumor samples and 59 normal samples. Patients with incomplete follow-up information and survival time less than 30 days were excluded to reduce statistical bias in the following analysis. A total of 472 LUAD patients were included in the further analysis. The mutation data of the included LUAD patients were also obtained from TCGA. For external validation, gene expression and clinical features of GSE31210 (N=226), GSE37745 (N=196), GSE50081 (N=181) were downloaded from GEO database (https://www.ncbi.nlm.nih.gov/geo/). They were integrated into a GEO meta-cohort for further analysis. To correct the batch effects and normalization, the R package 'sva' was used. Patients with other pathological types and survival time less than 30 days were excluded and finally 458 LUAD patients were included in the GEO meta-cohort. For subsequent models to be validated in the GEO meta-cohort, lncRNAs expressed in both TCGA and GEO datasets were identified. The clinical features of included LUAD patients in TCGA and GEO meta-cohort are shown in Table S1. Ethics approval was not required, as TCGA and GEO are public databases. The study was conducted in accordance with the Declaration of Helsinki (as revised in 2013).

Identification of CuRLs

Tsvetkov *et al.* recently discovered several genes essential for cuproptosis (4). Those genes identified in either Cu-DDC or elesclomol-Cu group were also included. In addition, the copper importer SLC31A1, copper exporters ATP7A/ATP7B, and lipoylated proteins were considered cuproptosis-related genes. Although experiments have demonstrated that Fe-S cluster proteins were downregulated after elesclomol treatment, the particular mechanism was unclear. Thus, Fe-S cluster proteins were not included in our analysis. Following that, Pearson correlation analysis was performed between cuproptosis-related genes and lncRNAs. Those lncRNAs with |correlation coefficient| >0.3 and P<0.001 were identified as CuRLs.

Establishment of the risk model

Combined with LUAD survival data from TCGA, univariate Cox regression was utilized to screen for prognostic cuproptosis-related lncRNAs. The lncRNAs with P<0.05 were further analyzed. Least Absolute Shrinkage and Selection Operator (LASSO) Cox regression as implemented in the R package 'glmnet' was then used to identify lncRNAs associated with the prognosis of LUAD with lambda.min as the cut-off. Stepwise multivariate Cox regression was further applied to examine the prognostic CuRLs. The stepwise approach was based on the Akaike information criterion (AIC) to define the optimal set of variables to retain in each model minimizing the AIC value (19). Finally, a 10-CuRLs signature was established. Each patient's risk score was calculated using the following formula:

$$Risk\ score = \sum_{i=1}^{n} Expression(lncRNA_n) \times Coefficient(lncRNA_n) \quad [1]$$

Bioinformatic analysis of identified CuRLs

The co-expression network was visualized by Cytoscape (version 3.9.1, http://www.cytoscape.org). Sankey diagram was obtained using the R package 'ggalluvial'. A heatmap of genes between tumor and normal samples was constructed by R package 'ComplexHeatmap' and 'circlize' (20,21).

Evaluation of the risk model

TCGA-LUAD patients were divided into low- and high-risk groups using the median risk score as the cut-off. Kaplan-Meier survival was applied to evaluate the differences in overall survival (OS) between the low- and high-risk patients. Univariate and multivariate Cox regression analyses were used to investigate whether the risk model based on identified cuproptosis-related lncRNAs was an independent risk factor considering other clinical signatures (age, gender, and stage) in LUAD patients. A predictive nomogram was developed using the R package 'rms'. The calibration curve and time-dependent receiver operating characteristic curve (ROC) were used to evaluate the predictive ability of the model. Principal component analysis (PCA) was performed to evaluate the grouping ability of the whole genome, cuproptosis genes, all CuRLs, and the identified 10-CuRLs signature.

External validation of the risk model

The GEO meta-cohort was considered a validation set to evaluate the model's performance. The risk score for each

patient was calculated by the same formula used for the TCGA cohort. Patients were also divided into low- and high-risk groups according to the median risk score. The risk model was analyzed to determine whether it was an independent prognostic factor in the validation cohort using similar methods in TCGA-LUAD training analysis.

Functional enrichment analysis

GSVA was applied to explore differences in enrichment scores between low-risk and high-risk groups, using pathways from the Molecular Signatures Database (MSigDB) hallmark set as a reference. GSEA was also performed for each lncRNA of the 10 CuRLs. The correlation between the expression of each lncRNA and other genes was computed. Gene lists were sorted by the value of correlation and then GSEA was performed based on KEGG pathway database with P value cutoff set to 0.05. Protein-coding genes co-expressed with the 10 CuRLs were identified using |Pearson correlation coefficient| >0.5 and P<0.001 as the cut-off. GO and KEGG functional enrichment analyses were carried out to understand the functions of these correlated mRNAs. These analyses were conducted mainly based on R packages 'GSVA', 'msigdbr', 'clusterProfiler' (22), 'org.Hs.eg.db', and 'enrichplot'.

Estimation of tumor immune microenvironment and TMB

Widely acknowledged methods were used for the evaluation of immune infiltration levels in LUAD patients, including the tumor immune estimation resource (TIMER), (23), cell-type identification by estimating relative subsets of RNA transcripts (CIBERSORT) (24), xCELL (25), QuanTIseq (26), microenvironment cell populations-counter (MCP-counter) (27), and estimating the proportions of immune and cancer cells (EPIC) algorithms (28). The Estimation of STromal and Immune cells in MAlignant Tumor tissues using Expression data (ESTIMATE) algorithm was also used to calculate the immune and stromal activity between low- and high-risk groups (29). To explore the differential expression of immune checkpoint genes (ICGs) between different risk patients, 79 ICGs were obtained from an article focusing on the roles of ICGs in predicting immunotherapy response (30). The R package 'maftools' was utilized to calculate the TMB of LUAD patients (31).

Significance of the CuRLs signature in drug sensitivity

To evaluate the differences in drug sensitivity between low- and high-risk groups, the R package 'pRRophetic' was applied which could yield a drug sensitivity for each patient based on the gene expression (32). The dataset 'cpg2016' in 'pRRophetic' included 251 types of drugs and we analyzed common anti-cancer drugs according to our clinical experience and review of related literature (18). The differences in drug sensitivity between low- and high-risk groups were represented by boxplots.

Statistical analysis

Data analysis was accomplished with R (version 4.1.2, the R Foundation for Statistical Computing, Vienna, Austria). Comparisons between 2 groups were evaluated using Wilcoxon test. Kruskal-Wallis test was used to evaluate the differences among more than 2 groups. A P<0.05 was considered significant.

Results

Identification of CuRLs in patients with LUAD

The flow chart in *Figure 1* depicts the primary design of our study. First, we identified 7,151 lncRNAs in LUAD samples from TCGA by excluding genes expressed in less than half of the cases. By intersecting these lncRNAs from TCGA and genes obtained in the GEO meta-cohort, 1,219 lncRNAs were identified for later investigation. Based on the excellent research by Tsvetkov *et al.* (4), we identified 17 cuproptosis-related genes (*ATP7A*, *ATP7B*, *CDKN2A*, *DBT*, *DLAT*, *DLD*, *DLST*, *FDX1*, *GCSH*, *GLS*, *LIAS*, *LIPT1*, *MTF1*, *PDHA1*, *PDHB*, *SLC31A1*, *LIPT2*) and retrieved their expression data in TCGA-LUAD. Then, 201 CuRLs were identified using Pearson correlation analysis (|correlation coefficient| >0.3 and P<0.001, Table S2). The co-expression network of cuproptosis-lncRNA was displayed as a Sankey diagram (*Figure 2A*).

Identification of prognostic CuRLs

Using univariate Cox regression, we identified 11 lncRNAs that were associated with poor prognosis and 25 lncRNAs that were associated with better survival outcomes (P<0.05, Table S3). LASSO Cox regression, as a common method of multiple regression method, can prevent overfitting and

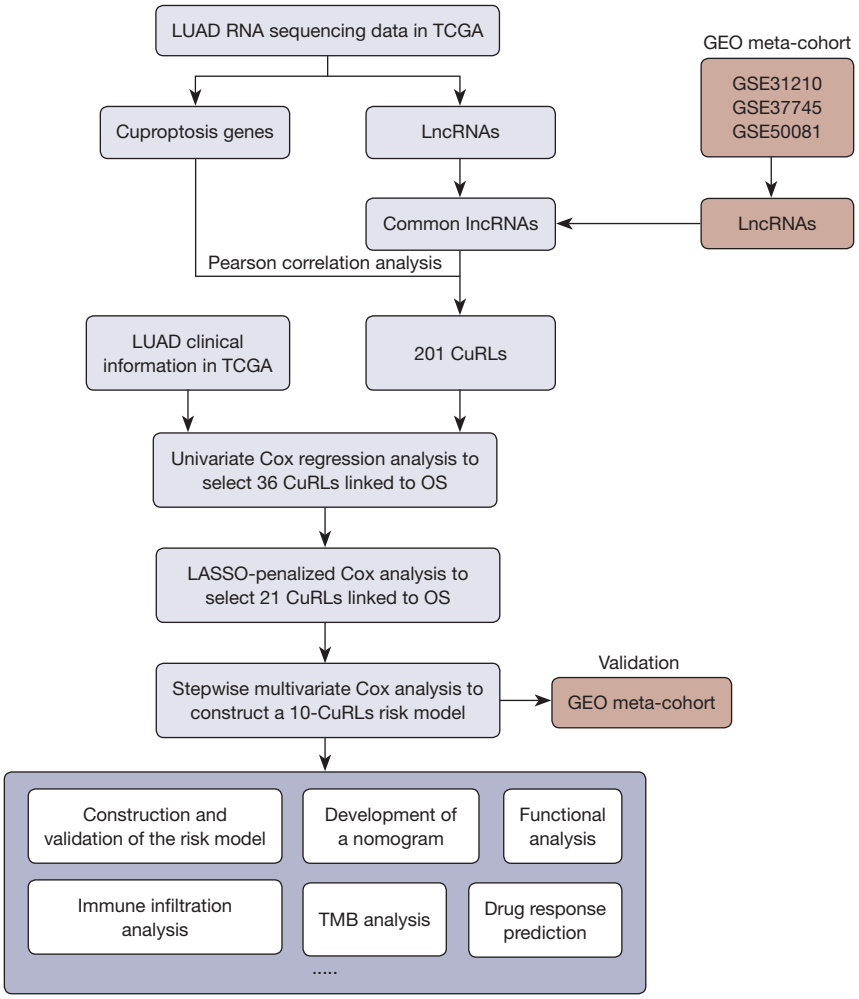

Figure 1 Flow chart of the present study. CuRLs, cuproptosis-related lncRNAs; LASSO, least absolute shrinkage and selection operator; LUAD, lung adenocarcinoma; OS, overall survival; TCGA, The Cancer Genome Atlas; TMB, tumor mutation burden.

enhance the generalization ability of the model by adding penalties. Using the lambda. min as the cut-off threshold, we identified 21 lncRNAs that significantly correlated to LUAD prognosis (*Figure 2B,2C*). Then, stepwise multivariate Cox analysis was used to analyze these lncRNAs, 10 of which were finally identified as a prognostic CuRLs signature (*Figure 2D*). *LINC01137* and *TMPO-AS1* were identified as poor prognostic factors, whereas *SEPSECS-AS1*, *CARD8-AS1*, and *ZSCAN16-AS1* were considered protective. The correlation between these 10 lncRNAs and cuproptosis genes is shown in *Figure 2E,2F*. We noted that most lncRNAs were both positively and negatively correlated with cuproptosis genes. Furthermore, we analyzed the correlations of the 10 CuRLs and found positive correlations between *APTR* and *ELOA-AS1*, *ZSCAN16-AS1* and *ELOA-SA1*, *SEPSECS-AS1* and *DLGAP1-AS1*, *SEPSECS-AS1* and *ELOA-AS1* (|correlation coefficient| >0.3 and P<0.05, *Figure 2G*). These indicated a complex regulatory network among cuproptosis genes and identified 10 CuRLs. We also examined the expression of these 10 CuRLs between normal and tumor tissues of LUAD (*Figure 2H*, Figure S1). *RUNDC3A-AS1*, *TMPO-AS1*, *ELOA-AS1*, *LINC01137*, *DLGAP1-AS1*, *MIR31HG*, and *APTR* were highly expressed in tumor samples, whereas the expression of *CARD8-AS1* was higher in normal tissues. The result suggested a role of these 10 CuRLs in classifying LUAD patients.

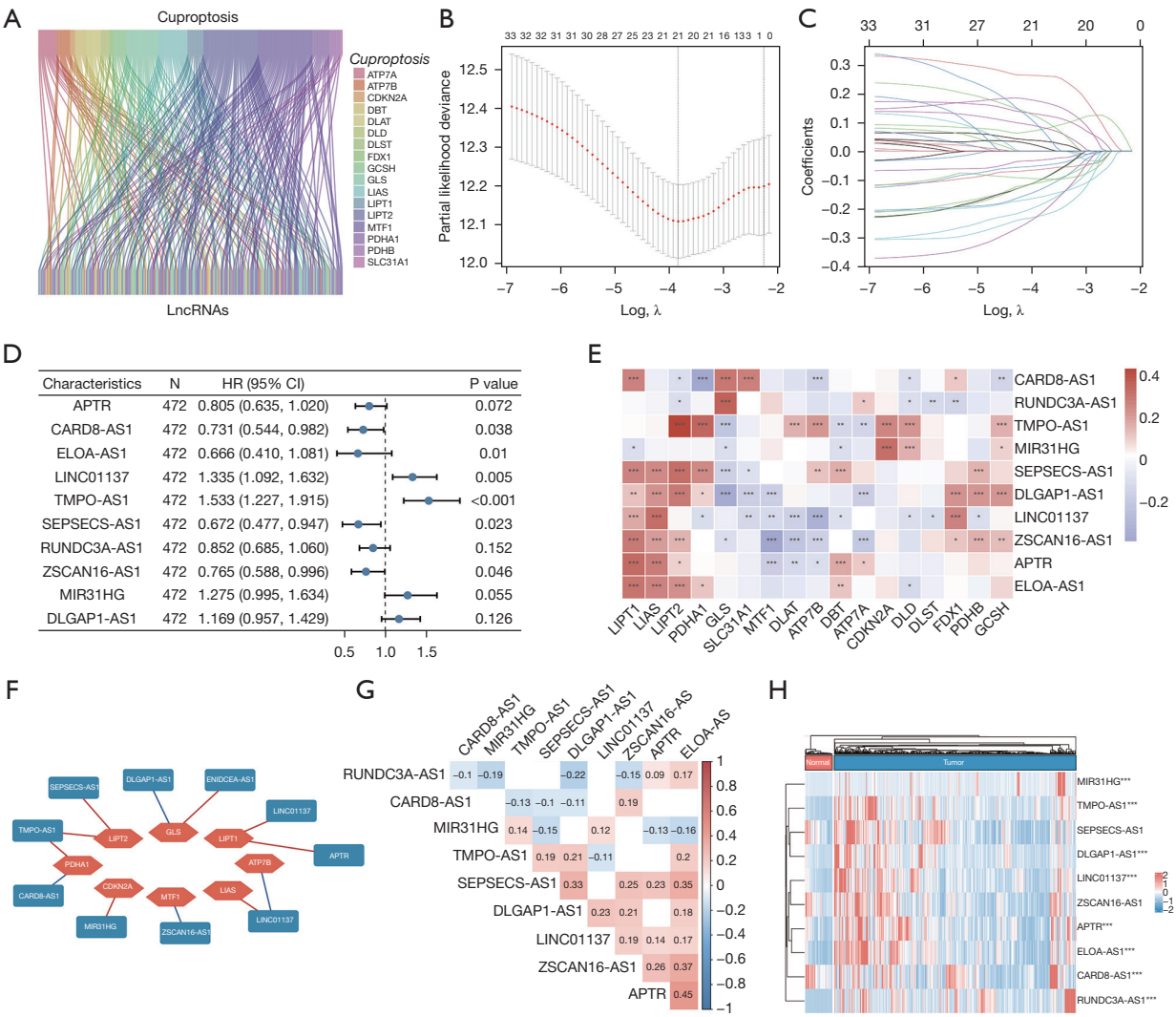

Figure 2 Identification of prognostic CuRLs in LUAD patients. (A) Sankey diagram for the cuproptosis genes and CuRLs. (B) Selection of tuning parameter lambda in the LASSO Cox regression model using ten-fold cross-validation. (C) LASSO coefficient profiles of 36 CuRLs. (D) Stepwise multivariate Cox regression analysis constructed a 10-CuRLs prognostic signature. (E) Heatmap for the correlation between cuproptosis genes and the 10 CuRLs. (F) A co-expression network of cuproptosis genes (orange diamond) and 10 CuRLs (blue rectangle). Red lines represent positive correlation, and blue lines represent negative correlation. (G) The correlation between the 10 CuRLs using Pearson analysis. Red squares represent positive correlation, blue squares represent negative correlation and white squares represent no significant correlation. (H) Hierarchical clustering for expression of the 10 CuRLs between normal and tumor samples. ***, P<0.001; **, P<0.01; *, P<0.05. CI, confidence interval; CuRLs, cuproptosis-related lncRNAs; HR, hazard ratio; LASSO, least absolute shrinkage and selection operator; LUAD, lung adenocarcinoma.

Construction and evaluation of the risk model based on prognostic CuRLs

The identified 10 prognostic CuRLs were used to construct a risk model. LUAD samples were divided into low-risk (N=236) and high-risk (N=236) groups with the median risk score as the threshold value. The distribution of the risk score and survival outcomes between the low-risk and high-risk groups are shown in *Figure 3A,3B*. The relative expression of the 10 prognostic CuRLs for each patient is shown in *Figure 3C*. The survival analysis demonstrated that the OS of the low-risk group was significantly longer than that of the high-risk group (P<0.001, *Figure 3D*). An

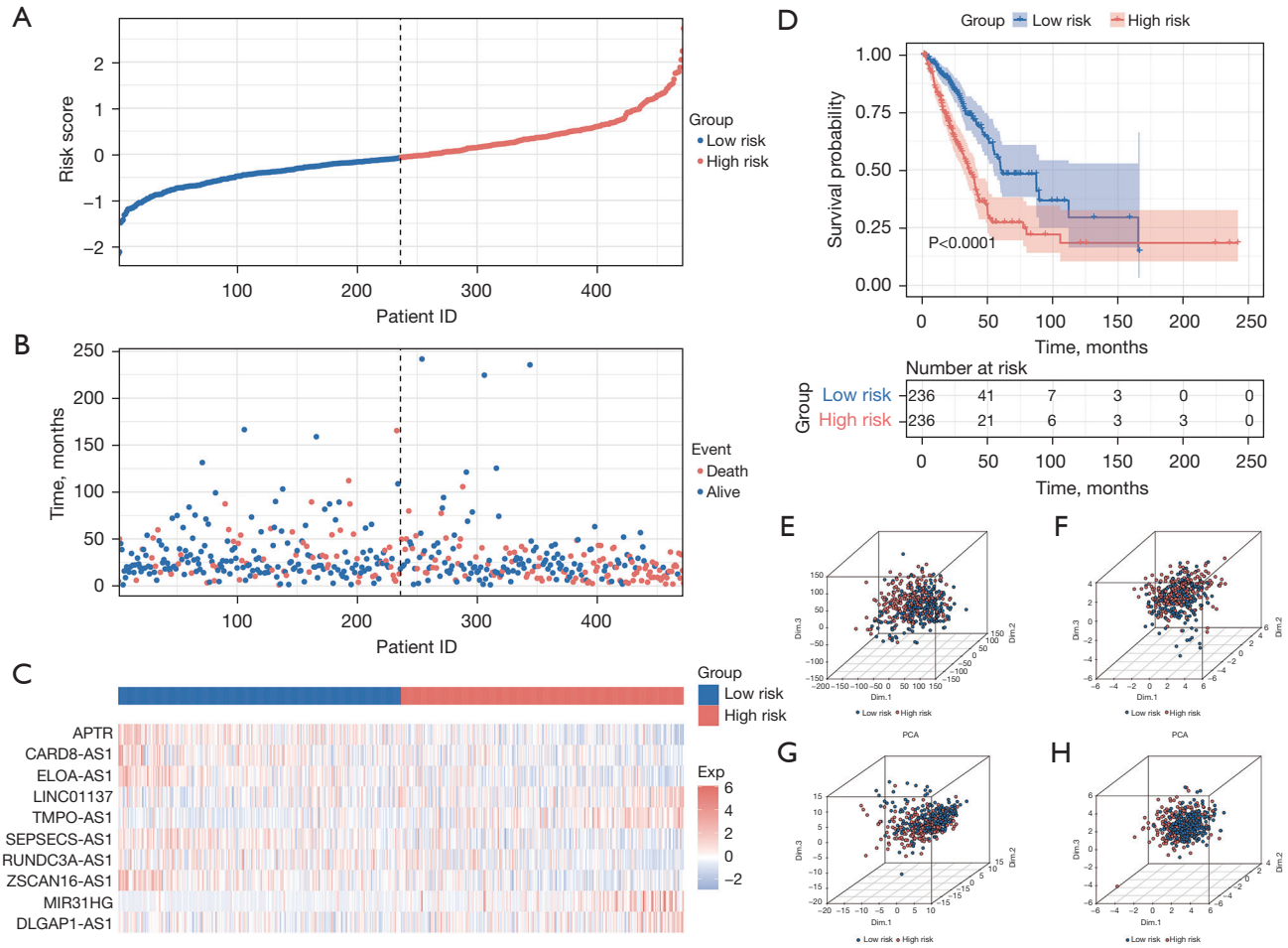

Figure 3 Prognostic value of the risk model based on 10 CuRLs. (A) Risk score distribution of patients in TCGA-LUAD cohort. (B) Survival status and time in the low- and high-risk groups. (C) Hierarchical clustering analysis of 10 CuRLs between the low- and high-risk groups. (D) Kaplan-Meier curve for OS in the low- and high-risk groups. Principal component analysis of low- and high-risk groups based on the whole-genome (E), cuproptosis genes (F) and all CuRLs (G). (H) The risk model based on 10 CuRLs. CuRLs, cuproptosis-related lncRNAs; LUAD, lung adenocarcinoma; OS, overall survival; TCGA, The Cancer Genome Atlas.

up-regulated expression of *ATPR*, *SEPSECS-AS1*, *ELOA-AS1*, *ZSCAN16-AS1*, *CARD8-AS1*, and *RUNDC3A-AS1* was observed in the low-risk group whereas the expression of *MIR31HG*, *TMPO-AS1*, *DLGAP1-AS1*, and *LINC01137* was higher in the high-risk group (Figure S2).

We conducted PCA to compare the low-risk and high-risk groups in order to verify the grouping capability of the risk model based on the identified 10 CuRLs. *Figure 3E-3H* display the distributions of low-risk and high-risk samples based on the entire genome, cuproptosis genes, all CuRLs, and the risk model. The results showed that the constructed risk model could distinguish the low-risk and high-risk patients much more effectively, indicating that the 10-CuRLs signature was a significant prognostic factor for LUAD patients.

Next, we performed univariate and multivariate Cox regression to evaluate the independence of the risk model based on the 10 CuRLs. The hazard ratio (HR) of the risk score was 2.718, and the 95% confidence interval (CI) was 2.179–3.391 (P<0.001) in the univariate Cox regression analysis (*Figure 4A*). In the multivariate Cox regression analysis, the HR of the risk score was 2.367 (95% CI: 1.892–2.963) (P<0.001), demonstrating that the 10-CuRLs signature was an independent prognostic factor (*Figure 4B*). A nomogram was constructed to assess the 1-, 3-, and 5-year OS incidences (*Figure 4C*). Calibration plots of the nomogram for 1-, 3-, and 5-years demonstrated the great

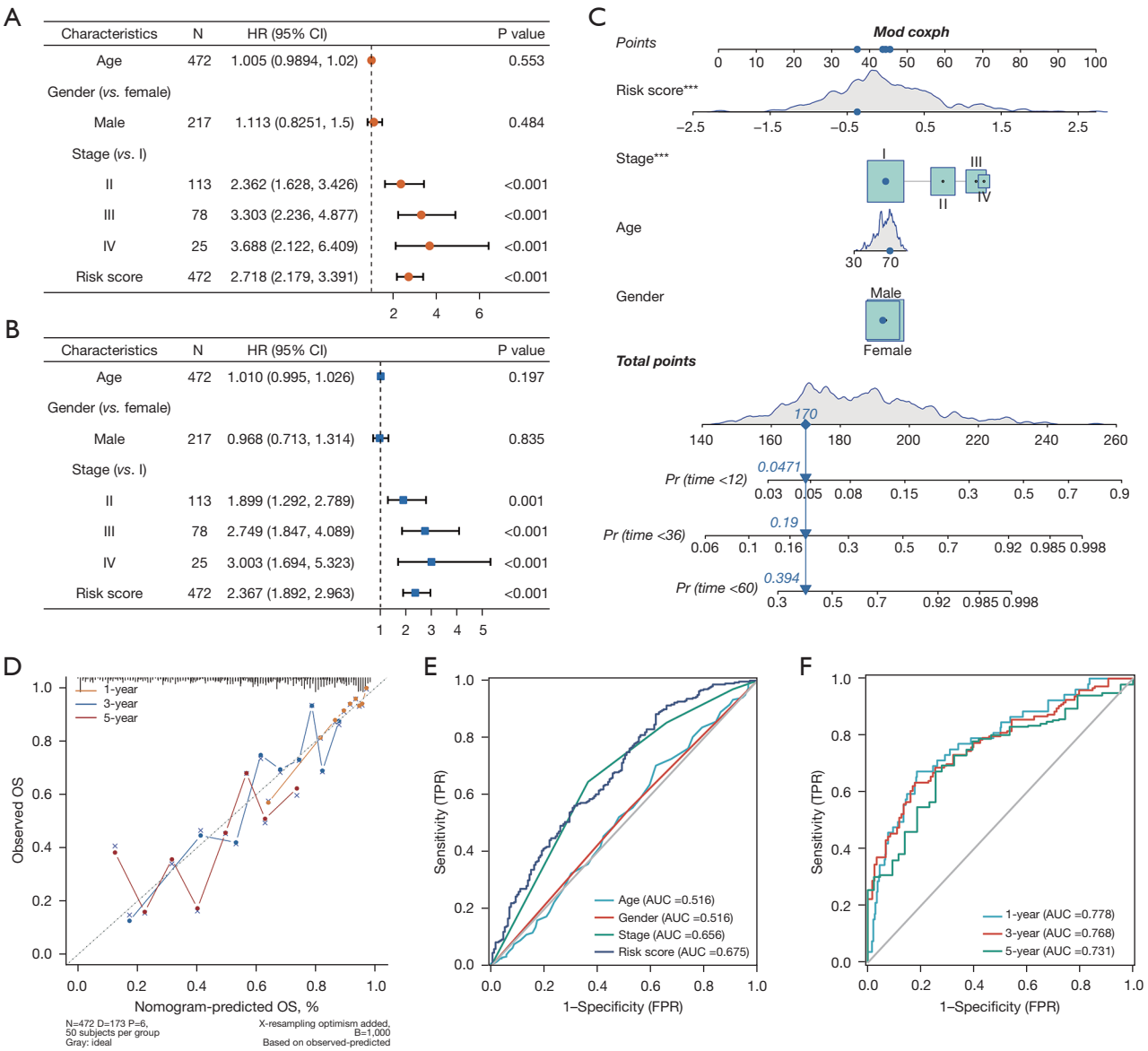

Figure 4 Independent prognostic analysis of the risk model. Forest plots showing (A) univariate and (B) multivariate Cox regression analysis of associations between clinical characteristics (including the 10-CuRLs signature) and OS. (C) A prognostic nomogram constructed to predict the 1-, 3-, and 5-year survival. (D) Calibration plot of the nomogram between the predicted and observed outcomes. (E) ROC curves of the clinical characteristics and risk score. (F) Time-dependent ROC curves of OS at 1-, 3- and 5-year. ***, P<0.001. AUC, area under the curve; CI, confidence interval; CuRLs, cuproptosis-related lncRNAs; HR, hazard ratio; OS, overall survival; ROC, receiver operating characteristic curve; TPR, true positive rate; FPR, false positive rate.

agreement between nomogram-predicted and observed results (*Figure 4D*). The area under the curve (AUC) values of the risk score, age, gender, and tumor stage are shown in *Figure 4E*, indicating the discriminative capability of the risk model with respect to LUAD survival. In addition, the AUC values at 1, 3, and 5 years reached 0.778, 0.768, and 0.731, respectively (*Figure 4F*).

Validation of the risk model as an independent prognostic factor for LUAD

To validate the risk model based on 10 prognostic CuRLs

obtained in the TCGA training cohort, we calculated risk scores for each patient in the GEO meta-cohort. Patients (N=458) were divided into low-risk and high-risk groups according to the median risk score. The distribution of risk score, survival outcome and expression of CuRLs are displayed in *Figure 5A-5C*. Kaplan-Meier survival analysis also showed that the OS of patients in the high-risk group was worse than that in the low-risk group (*Figure 5D*). We also included the risk model and clinical signatures in the univariate and multivariate Cox regression analysis (*Figure 5E,5F*). The univariate Cox regression analysis indicated that the 10-CuRLs signature was an independent prognostic factor (HR: 1.468, 95% CI: 1.331–1.620, P<0.001). The associations between the risk score and OS remained significant after adjusting for potential confounding factors in the multivariate Cox regression analysis (HR: 1.398, 95% CI: 1.258–1.553, P<0.001). The risk score showed better discriminatory ability over other clinical features (*Figure 5G*). The predictive accuracy was also evaluated by time-dependent ROC analysis, and the AUC value of 1-, 3-, and 5-year reached 0.765, 0.751, and 0.709, respectively (*Figure 5H*). These results demonstrated that the 10-CuRLs signature had a good-prognostic value in both TCGA training cohort and GEO validation meta-cohort.

Identification of the 10 CuRLs-associated biological pathways

We used different approaches to fully explore biological functions associated with the risk model based on the 10 CuRLs. We applied GSVA to identify biological processes that differed significantly between low- and high-risk groups (*Figure 6A*). Many cancer-related pathways were differentially enriched between the two risk groups, such as glycolysis, p53 pathway, MTORC1 signaling, and apoptosis. The low-risk group showed enrichment for inflammatory response and angiogenesis. We then performed GSEA analysis for each lncRNA of the 10 CuRLs based on the KEGG pathway database. These CuRLs were enriched in pathways associated with cell death and immunity, as shown in GSEA enrichment plots of *APTR* and *CARD8-AS1* (*Figure 6B,6C*). Figure S3 delineated the top 5 differentially regulated pathways of *DLGAP1-AS1*, *ELOA-AS1*, *LINC01137*, *MIR31HG*, *TMPO-AS1*, and *ZSCAN16-AS1* (all pathways and their GSEA enrichment scores were not shown). These results indicated potential links between CuRLs and other types of cell death, such as apoptosis, ferroptosis, and necroptosis. In addition, these lncRNAs tended to be involved in immune-associated pathways, such as programmed death ligand-1 (PD-L1) expression and programmed cell death protein 1 (PD-1) checkpoint pathway in cancer, T cell receptor signaling pathway, and antigen processing and presenting. Protein-coding genes co-expressed with the 10 CuRLs were identified using |Pearson correlation coefficient| >0.5 and P<0.001 as the cut-off (Table S4). GO and KEGG analyses were then performed based on these correlated messenger RNAs (mRNAs). The results showed that the 10 CuRL-related mRNAs were enriched in immune receptor activity, T cell activation, and T cell receptor signaling pathway (*Figure 6D,6E*). These results suggested that the 10-CuRLs signature was not only relevant to traditional cancer-related pathways but also associated with immune response.

Evaluation of tumor-immune landscape and TMB based on the risk model

To explore the roles of the risk model based on the 10 CuRLs in TIME, we evaluated the landscape of immune cell infiltration in tumor samples. Infiltration levels of immune cells between low- and high-risk groups were calculated by TIMER, CIBERSORT, QuanTIseq, MCP-counter, xCELL, and EPIC algorithms (*Figure 7* and Table S5). In low-risk samples, multiple immune cells were highly expressed, including B cells and CD4+ T cells. According to the xCELL algorithm, we observed more types of infiltrated immune cells in low-risk samples, such as activated myeloid dendritic cells, CD8+ T cells, monocytes, and so on. We found that the risk score was negatively related to the immune and stroma scores based on the xCELL algorithm, suggesting that increased risk may lead to fewer intra-tumoral immune cells. However, a significant difference in stromal activity was not observed based on the ESTIMATE algorithm (*Figure 8A,8B*). Considering the development of ICIs, we further examined the expression of 79 ICGs between low- and high-risk groups, and 36 of them were found to be differentially expressed (*Figure 8C*). Notably, there was a significant difference in CTLA4, which is dysregulated in tumors and tumor-associated T cells and is a promising immunotherapeutic target. The higher expression of CTLA4 in low-risk patients indicated that these patients may be more likely to benefit from anti-CTLA4 treatment. The relation between the risk group and CD276 also attracted our attention. CD276 has been recently discovered to enable cancer stem cells to evade immune surveillance (33). The high expression of CD276

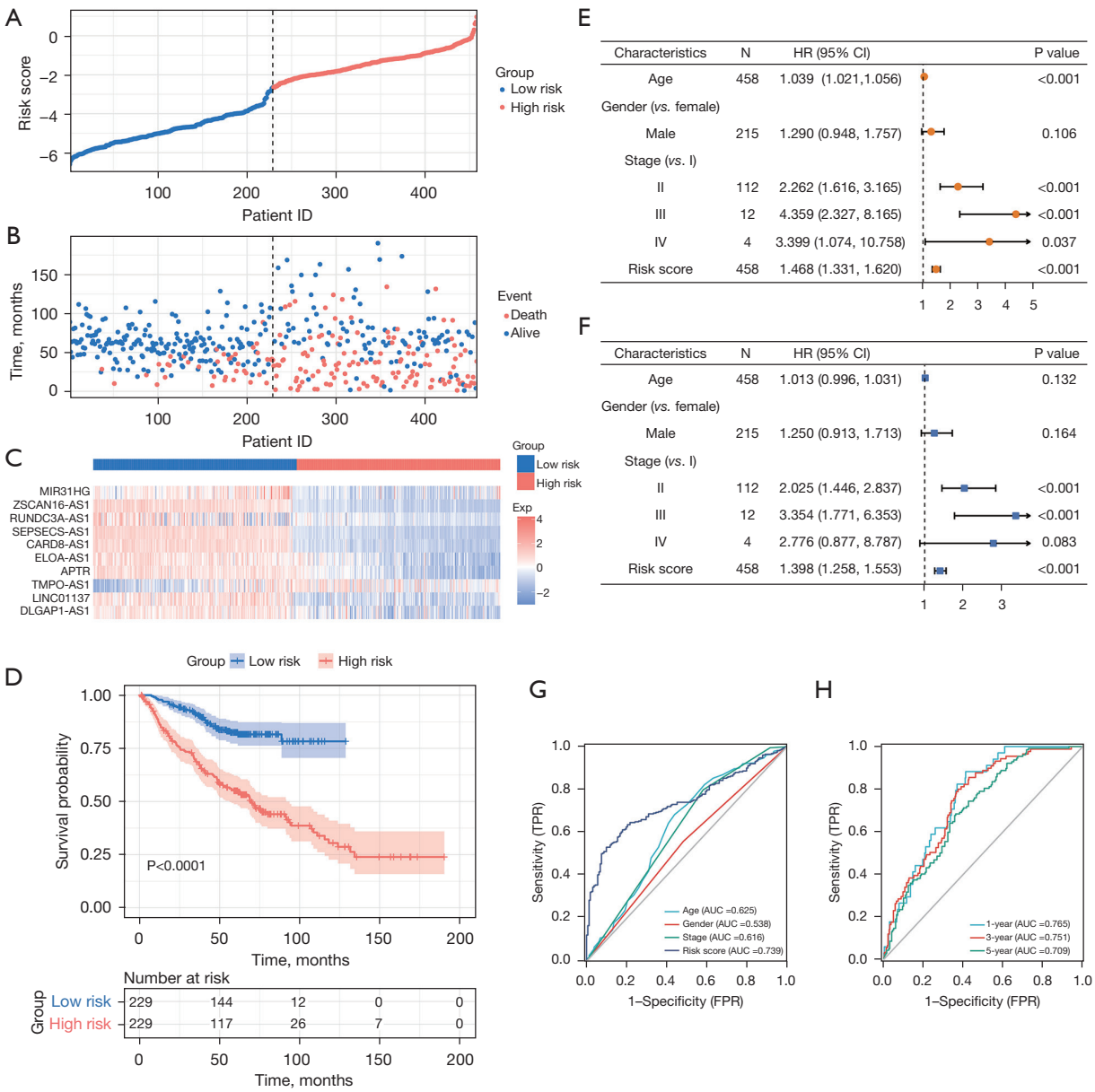

Figure 5 Validation of the risk model in the GEO cohort. (A) Distribution of 10-CuRLs risk model-based risk score in the GEO meta-cohort. (B) Survival status and time in the low- and high-risk groups. (C) Hierarchical clustering analysis of 10 CuRLs between the low- and high-risk groups. (D) Kaplan-Meier curve for OS in the low- and high-risk groups. Forest plots showing univariate (E) and multivariate (F) Cox regression analysis of associations between clinical characteristics (including the 10-CuRLs signature) and OS. (G) ROC curves of the clinical characteristics and risk score. (H) Time-dependent ROC curves of OS at 1-, 3- and 5-year. AUC, area under the curve; CI, confidence interval; CuRLs, cuproptosis-related lncRNAs; HR, hazard ratio; OS, overall survival; ROC, receiver operating characteristic curve; TPR, true positive rate; FPR, false positive rate.

in high-risk groups indicted that immune suppression in TIME of high-risk samples could permit tumor cells to escape, leading to drug resistance. The correlation heatmap also showed significant associations between risk score and ICGs (*Figure 8D*).

Emerging evidence suggests that TMB is a biomarker

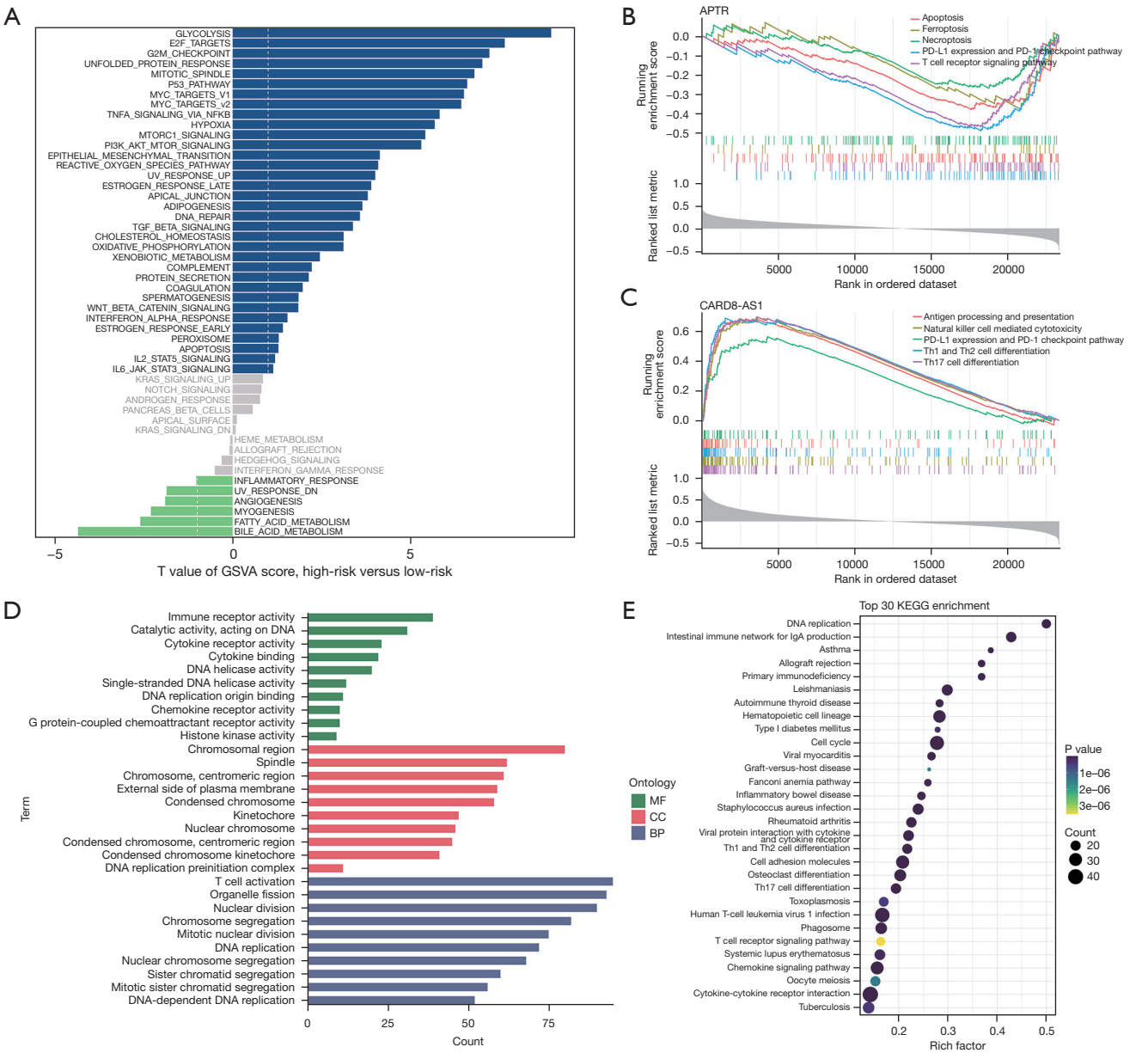

Figure 6 Functional analysis of the risk model based on 10 CuRLs. (A) GSVA analysis between low- and high-risk groups. GSEA analysis based on KEGG pathway database of lncRNA (B) *APTR* and (C) *CARD8-AS1*. (D) GO enrichment analysis of CuRLs-related mRNAs. (E) KEGG pathway enrichment analysis of CuRLs-related mRNAs. BP, biological process; CC, cellular component; CuRLs, cuproptosis-related lncRNA; GO, Gene Ontology; GSEA, gene set enrichment analysis; GSVA, gene set variation analysis; KEGG, Kyoto Encyclopedia of Genes and Genomes; MF, molecular function; PD-1, programmed death-1; PD-L1, programmed cell death-ligand 1; Th 1/2/17, T helper cell 1/2/17.

of response to ICI treatment (34). Therefore, we explored the differences in TMB between low- and high-risk groups. It was found that patients in the high-risk group exhibited a higher TMB compared with the low-risk group (*Figure 8E*). Higher TMB was associated with a favorable prognosis in LUAD patients (*Figure 8F*). Intriguingly, the two results appear to contradict the poor prognosis in high-risk groups. Thus, we divided patients into 4 groups based on TMB and

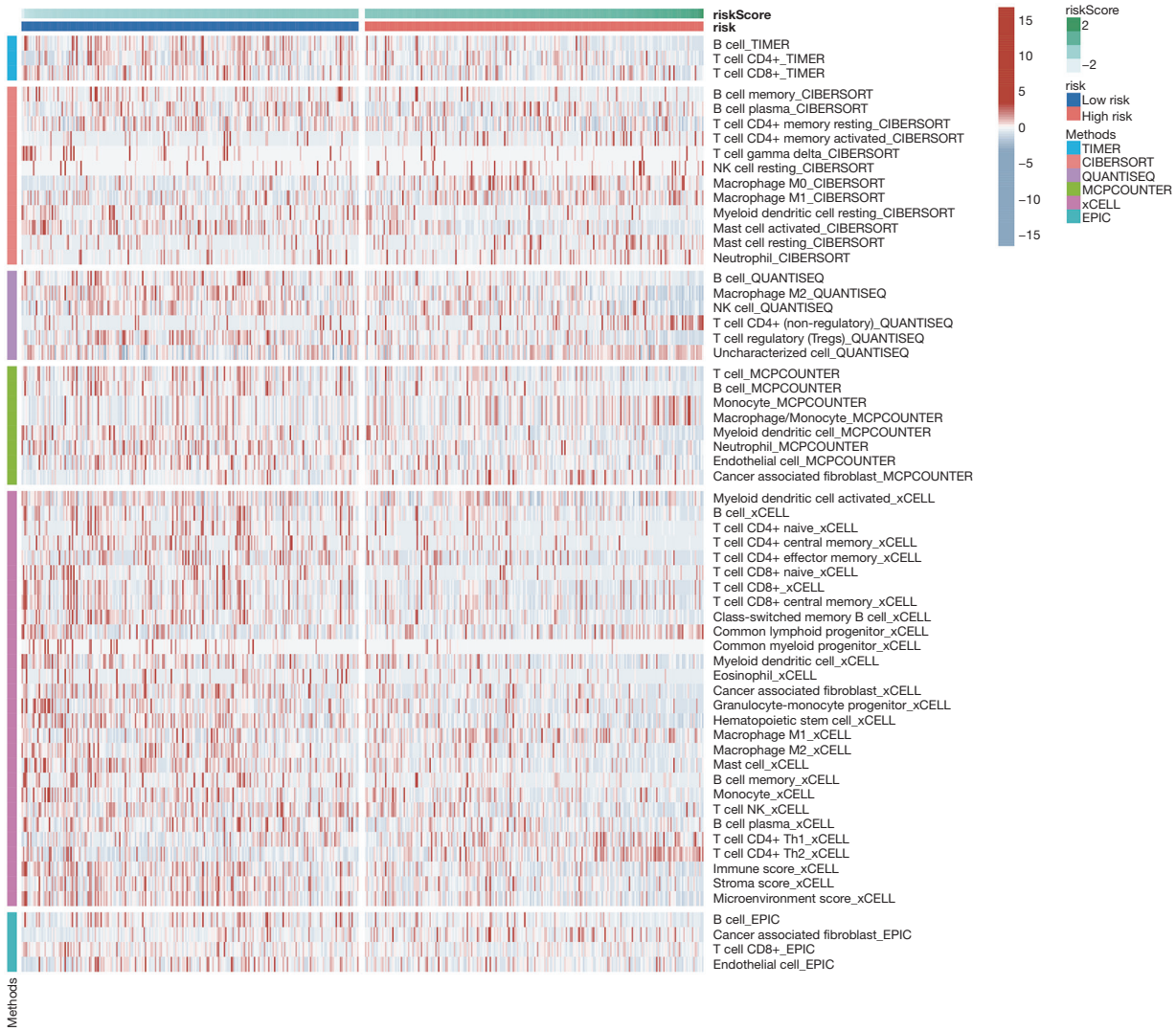

Figure 7 Comparisons of infiltrated immune cells between low-risk and high-risk groups based on TIMER, CIBERSORT, QUANTISEQ, MCP-counter, xCELL, and EPIC algorithms. CIBERSORT, cell-type identification by estimating relative subsets of RNA transcripts; EPIC, estimating the proportions of immune and cancer cells; MCP-counter, microenvironment cell populations-counter; TIMER, tumor immune estimation resource.

risk score (*Figure 8G*). Patients with a low TMB and high risk score had the least favorable OS. Correspondingly, low-risk patients with a high TMB had the best prognosis. These results indicated that risk group combined with TMB might provide a more precise assessment of patient prognosis.

Comparison of the sensitivity to anti-cancer drugs between low- and high-risk patients

The different landscape of TIME and TMB may lead to differential susceptibility to drug response. Therefore, we utilized the pRRophetic algorithm to detect suitable targeted drugs for patients in low- and high-risk groups. The sensitivity of 15 drugs that are currently in clinical use or in preclinical trials for lung cancer showed significant differences between low- and high-risk groups ($P<0.05$, *Figure 9A*). Among drugs commonly used in the treatment of non-small cell lung cancer clinically, the sensitivity of cisplatin, docetaxel, gemcitabine, gefitinib, and paclitaxel was higher in patients with low risk (*Figure 9B-9G*), suggesting that these drugs may be more effective in high-risk patients. However, low-risk patients might benefit more

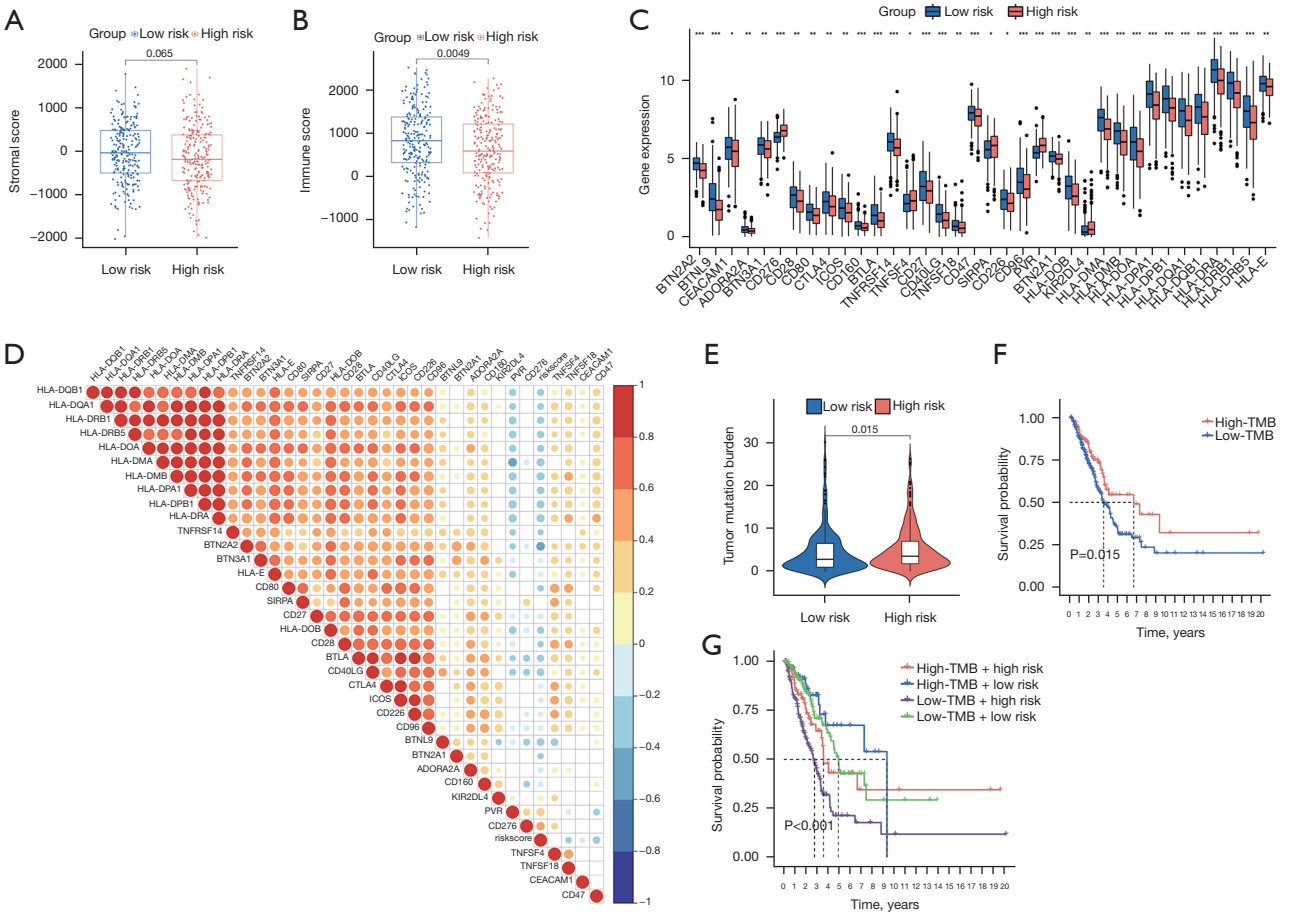

Figure 8 Differences in the TIME between low- and high-risk groups. (A,B) Comparison of the stromal score and immune score between low- and high-risk samples. (C) The differential expression of ICGs in low- and high-risk groups. (D) Correlation heatmap showing the associations between risk score and ICGs. White squares represent no significant correlation. (E) Comparison of TMB between low- and high-risk groups. (F) Kaplan-Meier analysis of the effect of TMB status on OS. (G) Kaplan-Meier analysis for OS of patients categorized by combing TMB status and risk score. ICG, immune checkpoint gene; OS, overall survival; TIME, tumor immune microenvironment; TMB, tumor mutation burden.

from imatinib. Some other drugs in preclinical use also exhibited potential for lung cancer treatment in different risk groups (Figure S4).

Discussion

Despite progress made in the field of surgery, chemotherapy, radiotherapy, and immunotherapy, the current status of LUAD treatment is far from satisfactory. Novel molecular biomarkers, which could provide additional prognostic value and better risk assessment, may help clinicians to develop personalized therapy.

Various types of PCD, such as necroptosis, pyroptosis, and ferroptosis, have shown vital roles in inhibiting cancer progression and clinical deterioration (35-38). Although the introduction of ICI represents a milestone in cancer treatment, only one-third of patients are responsive (39). The activation of cell death has also been discovered to boost the efficacy of anti-tumor immune therapy (3). For example, the acute activation of pyroptosis leads to the release of inflammatory cytokines and immunostimulatory alarmins, thus increasing the infiltration of various immune cells (40). Wang *et al.* found that pyroptosis could turn 'cold' tumors into 'hot' tumors and exhibited an anti-tumor effect synergistically with ICI (41).

Copper binding agents acting as copper ionophores have

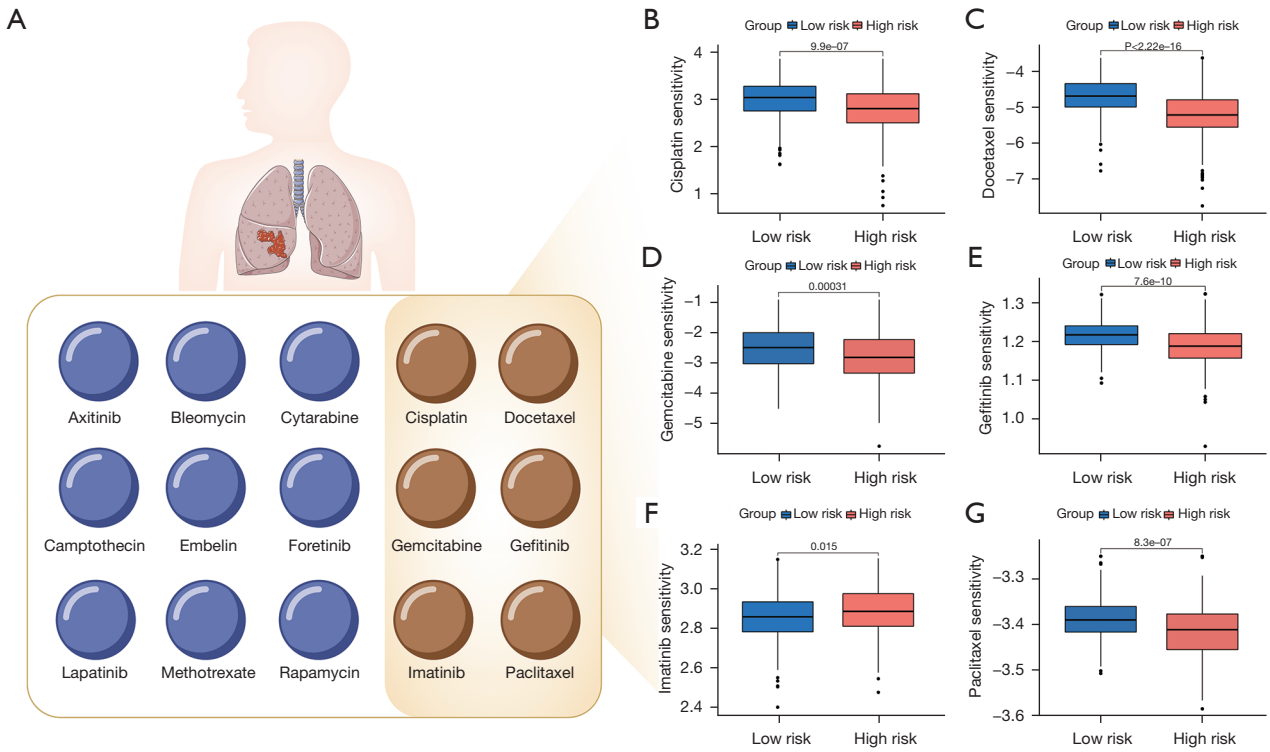

Figure 9 Predicted drug responses in low- and high-risk groups. (A) Schematic diagram for anti-cancer drugs currently in clinical use or in preclinical trials for lung cancer (P<0.05). Differences in drug sensitivity of (B) Cisplatin, (C) Docetaxel, (D) Gemcitabine, (E) Gefitinib, (F) Imatinib, (G) Paclitaxel.

been found to lead to cell death in tumor cells and provided a rationale for the exploitation of copper toxicity as an anti-tumor tool (42). However, the molecular mechanism of the induction of copper and its role in anti-tumor activity is still unclear. A novel type of cell death, cuproptosis mediated by protein lipoylation has been recently elucidated, opening the door for cuproptosis as a novel approach in cancer treatment (4).

The role of lncRNAs in PCD cannot be ignored (15). The overexpression of lncRNA *LINC0036* up-regulated cystathionine β synthase (CBS) which is a ferroptosis marker in lung cancer cells (43). It suggests that combining lncRNAs with PCD may lead to a better understanding of the underlying tumor biology. Several recent studies constructed clinical models based on PCD-related lncRNAs to predict the prognosis and immune response of patients (17,18,44,45). Therefore, it is quite worthy to explore the prognostic value of CuRLs in LUAD, which is a new hotspot in the field of cell death. In this study, using Cox regression analysis and a machine-learning algorithm based on LASSO analysis, we developed a novel 10-CuRLs signature to predict patient prognosis combined with conventional clinical risk factors. The CuRLs signature showed great prediction accuracy, which was further validated in a GEO meta-cohort.

A number of studies have focused on the crosstalk between cell death and TIME (3,46,47). In our research, we also fully explored the biological functions associated with the risk model based on the 10 CuRLs. It was found that the 10 CuRLs-related mRNAs were enriched in immune receptor activity, T cell activation, and T cell receptor signaling pathway. These results suggested that the 10-CuRLs signature was not only relevant to traditional cancer-related pathways but also associated with immune response. Therefore, we further evaluated the tumor-immune landscape based on our CuRLs risk mode and sequentially observed significant differences in the immune landscape between low-risk and high-risk groups. This may guide clinicians in making individualized treatment decisions between different risk groups.

Multiple differentially expressed ICGs between low- and high-risk groups bring about new prospects for the

administration of ICIs for LUAD patients with different risk scores. In addition to CTLA4 and CD276 already mentioned above, some other ICGs are worthy of attention. Butyrophilins (BTNs), which are structurally similar to the immunosuppressive B7 family, are of great importance in restarting the anti-tumor efficacy of γδ T cells (48,49). The higher expression of BTN2A1, BTN2A2, and BTNL9 in the low-risk group indicated that these patients may have a better response to checkpoint immunotherapy. In low-risk patients, we also observed higher expression of genes in HLA class II which could present antigens to CD4+ T cells (50,51). These HLA-II genes hold promise as a predictive biomarker of response to anti-PD-1 or anti-PD-L1 therapy (52).

TMB, defined as the number of somatic mutations per megabase, is emerging as a potential biomarker for the response to immunotherapy (53). However, there is currently no consensus over the optimal cut-off of TMB for patient stratification, leading to limited further application in the clinic (54). In our present study, the combination of TMB and the CuRLs risk model brought about a more accurate analysis of patient survival, indicating that TMB combined with the CuRLs risk model may serve as a promising prognostic factor in addition to predicting the immune response. Our study further showed the ability of the CuRLs risk model to predict the sensitivity to anti-cancer drugs, which may provide a novel method for clinical medication-related decisions.

Although our findings have been validated in an independent meta-cohort, our study had some limitations. On the one hand, our study was retrospective based on publicly available TCGA and GEO databases and these results need to be verified in prospective studies for clinical use. On the other hand, further biological experiments are needed to confirm the expression of these key genes and elucidate their biological functions in lung cancer.

Conclusions

To our knowledge, the present study is the first to construct a CuRLs prognostic signature in patients with LUAD and validate it in an external meta-cohort. The risk model exhibited a high diagnostic accuracy in predicting patient survival outcomes combined with clinical features. The differences in characteristics between low- and high-risk groups, including immune infiltration, TMB, and drug sensitivity, open the way to better patient stratification and explore novel drugs in different risk groups. We are looking forward to furthering studies into the mechanisms behind how these CuRLs regulate cuproptosis and affect patient outcomes. We hope the CuRLs risk model could be validated in more clinical cohorts and further benefit patients in the future.

Acknowledgments

We thank Dr. Jianming Zeng (University of Macau), and all the members of his bioinformatics team, biotrainee, for generously sharing their experience and codes. We also would like to acknowledge the work by TCGA, GSE31210, GSE37745, and GSE50081 for providing LUAD data.

Funding: This work was supported by the National Natural Science Foundation of China (No. 82072557 to HL, No. 81871882 to HL, No. 82001976 to HJ); National Key Research and Development Program of China (No. 2021YFC2500900 to HL); Shanghai Municipal Education Commission- Gaofeng Clinical Medicine Grant (No. 20172005, the 2nd round of disbursement to HL); Program of Shanghai Academic Research Leader from Science and Technology Commission of Shanghai Municipality (No. 20XD1402300 to HL); and Shanghai Sailing Program (No. 20YF1440000 to HJ).

Footnote

Reporting Checklist: The authors have completed the TRIPOD reporting checklist. Available at https://tlcr.amegroups.com/article/view/10.21037/tlcr-22-500/rc

Peer Review File: Available at https://tlcr.amegroups.com/article/view/10.21037/tlcr-22-500/prf

Conflicts of Interest: All authors have completed the ICMJE uniform disclosure form (available at https://tlcr.amegroups.com/article/view/10.21037/tlcr-22-500/coif). The authors have no conflicts of interest to declare.

Ethical Statement: The authors are accountable for all aspects of the work in ensuring that questions related to the accuracy or integrity of any part of the work are appropriately investigated and resolved. The study was conducted in accordance with the Declaration of Helsinki (as revised in 2013).

References

1. Siegel RL, Miller KD, Fuchs HE, et al. Cancer statistics, 2022. CA Cancer J Clin 2022;72:7-33.
2. Snyder AG, Oberst A. The Antisocial Network: Cross Talk Between Cell Death Programs in Host Defense. Annu Rev Immunol 2021;39:77-101.
3. Tang R, Xu J, Zhang B, et al. Ferroptosis, necroptosis, and pyroptosis in anticancer immunity. J Hematol Oncol 2020;13:110.
4. Tsvetkov P, Coy S, Petrova B, et al. Copper induces cell death by targeting lipoylated TCA cycle proteins. Science 2022;375:1254-61.
5. Kim BE, Nevitt T, Thiele DJ. Mechanisms for copper acquisition, distribution and regulation. Nat Chem Biol 2008;4:176-85.
6. Williams DM. Copper deficiency in humans. Semin Hematol 1983;20:118-28.
7. Oliveri V. Selective Targeting of Cancer Cells by Copper Ionophores: An Overview. Front Mol Biosci 2022;9:841814.
8. Margalioth EJ, Schenker JG, Chevion M. Copper and zinc levels in normal and malignant tissues. Cancer 1983;52:868-72.
9. Yu Z, Zhou R, Zhao Y, et al. Blockage of SLC31A1-dependent copper absorption increases pancreatic cancer cell autophagy to resist cell death. Cell Prolif 2019;52:e12568.
10. Yao W, Qian X, Ochsenreither S, et al. Disulfiram Acts as a Potent Radio-Chemo Sensitizer in Head and Neck Squamous Cell Carcinoma Cell Lines and Transplanted Xenografts. Cells 2021;10:517.
11. Volders PJ, Anckaert J, Verheggen K, et al. LNCipedia 5: towards a reference set of human long non-coding RNAs. Nucleic Acids Res 2019;47:D135-9.
12. Chen J, Zhang K, Zhi Y, et al. Tumor-derived exosomal miR-19b-3p facilitates M2 macrophage polarization and exosomal LINC00273 secretion to promote lung adenocarcinoma metastasis via Hippo pathway. Clin Transl Med 2021;11:e478.
13. Qian X, Yang J, Qiu Q, et al. LCAT3, a novel m6A-regulated long non-coding RNA, plays an oncogenic role in lung cancer via binding with FUBP1 to activate c-MYC. J Hematol Oncol 2021;14:112.
14. Loewen G, Jayawickramarajah J, Zhuo Y, et al. Functions of lncRNA HOTAIR in lung cancer. J Hematol Oncol 2014;7:90.
15. Jiang N, Zhang X, Gu X, et al. Progress in understanding the role of lncRNA in programmed cell death. Cell Death Discov 2021;7:30.
16. Tanzhu G, Li N, Li Z, et al. Molecular Subtypes and Prognostic Signature of Pyroptosis-Related lncRNAs in Glioma Patients. Front Oncol 2022;12:779168.
17. Guo Y, Qu Z, Li D, et al. Identification of a prognostic ferroptosis-related lncRNA signature in the tumor microenvironment of lung adenocarcinoma. Cell Death Discov 2021;7:190.
18. Tang R, Wu Z, Rong Z, et al. Ferroptosis-related lncRNA pairs to predict the clinical outcome and molecular characteristics of pancreatic ductal adenocarcinoma. Brief Bioinform 2022;23:bbab388.
19. Zeidan AM, Sekeres MA, Garcia-Manero G, et al. Comparison of risk stratification tools in predicting outcomes of patients with higher-risk myelodysplastic syndromes treated with azanucleosides. Leukemia 2016;30:649-57.
20. Gu Z, Eils R, Schlesner M. Complex heatmaps reveal patterns and correlations in multidimensional genomic data. Bioinformatics 2016;32:2847-9.
21. Gu Z, Gu L, Eils R, et al. circlize Implements and enhances circular visualization in R. Bioinformatics 2014;30:2811-2.
22. Wu T, Hu E, Xu S, et al. clusterProfiler 4.0: A universal enrichment tool for interpreting omics data. Innovation (Camb) 2021;2:100141.
23. Li T, Fu J, Zeng Z, et al. TIMER2.0 for analysis of tumor-infiltrating immune cells. Nucleic Acids Res 2020;48:W509-14.
24. Newman AM, Liu CL, Green MR, et al. Robust enumeration of cell subsets from tissue expression profiles. Nat Methods 2015;12:453-7.
25. Aran D, Hu Z, Butte AJ. xCell: digitally portraying the tissue cellular heterogeneity landscape. Genome Biol 2017;18:220.
26. Finotello F, Mayer C, Plattner C, et al. Molecular and pharmacological modulators of the tumor immune contexture revealed by deconvolution of RNA-seq data. Genome Med 2019;11:34.
27. Becht E, Giraldo NA, Lacroix L, et al. Estimating the

population abundance of tissue-infiltrating immune and stromal cell populations using gene expression. Genome Biol 2016;17:218.
28. Racle J, Gfeller D. EPIC: A Tool to Estimate the Proportions of Different Cell Types from Bulk Gene Expression Data. Methods Mol Biol 2020;2120:233-48.
29. Yoshihara K, Shahmoradgoli M, Martínez E, et al. Inferring tumour purity and stromal and immune cell admixture from expression data. Nat Commun 2013;4:2612.
30. Hu FF, Liu CJ, Liu LL, et al. Expression profile of immune checkpoint genes and their roles in predicting immunotherapy response. Brief Bioinform 2021;22:bbaa176.
31. Mayakonda A, Lin DC, Assenov Y, et al. Maftools: efficient and comprehensive analysis of somatic variants in cancer. Genome Res 2018;28:1747-56.
32. Geeleher P, Cox N, Huang RS. pRRophetic: an R package for prediction of clinical chemotherapeutic response from tumor gene expression levels. PLoS One 2014;9:e107468.
33. Wang C, Li Y, Jia L, et al. CD276 expression enables squamous cell carcinoma stem cells to evade immune surveillance. Cell Stem Cell 2021;28:1597-1613.e7.
34. Offin M, Rizvi H, Tenet M, et al. Tumor Mutation Burden and Efficacy of EGFR-Tyrosine Kinase Inhibitors in Patients with EGFR-Mutant Lung Cancers. Clin Cancer Res 2019;25:1063-9.
35. Friedmann Angeli JP, Krysko DV, Conrad M. Ferroptosis at the crossroads of cancer-acquired drug resistance and immune evasion. Nat Rev Cancer 2019;19:405-14.
36. Jiang X, Stockwell BR, Conrad M. Ferroptosis: mechanisms, biology and role in disease. Nat Rev Mol Cell Biol 2021;22:266-82.
37. Gong Y, Fan Z, Luo G, et al. The role of necroptosis in cancer biology and therapy. Mol Cancer 2019;18:100.
38. Xia X, Wang X, Cheng Z, et al. The role of pyroptosis in cancer: pro-cancer or pro-"host"? Cell Death Dis 2019;10:650.
39. Jiang P, Gu S, Pan D, et al. Signatures of T cell dysfunction and exclusion predict cancer immunotherapy response. Nat Med 2018;24:1550-8.
40. Du T, Gao J, Li P, et al. Pyroptosis, metabolism, and tumor immune microenvironment. Clin Transl Med 2021;11:e492.
41. Wang Q, Wang Y, Ding J, et al. A bioorthogonal system reveals antitumour immune function of pyroptosis. Nature 2020;579:421-6.
42. Tardito S, Bassanetti I, Bignardi C, et al. Copper binding agents acting as copper ionophores lead to caspase inhibition and paraptotic cell death in human cancer cells. J Am Chem Soc 2011;133:6235-42.
43. Wang M, Mao C, Ouyang L, et al. Long noncoding RNA LINC00336 inhibits ferroptosis in lung cancer by functioning as a competing endogenous RNA. Cell Death Differ 2019;26:2329-43.
44. Ye Y, Dai Q, Qi H. A novel defined pyroptosis-related gene signature for predicting the prognosis of ovarian cancer. Cell Death Discov 2021;7:71.
45. Yao J, Chen X, Liu X, et al. Characterization of a ferroptosis and iron-metabolism related lncRNA signature in lung adenocarcinoma. Cancer Cell Int 2021;21:340.
46. Loveless R, Bloomquist R, Teng Y. Pyroptosis at the forefront of anticancer immunity. J Exp Clin Cancer Res 2021;40:264.
47. Zeng Q, Ma X, Song Y, et al. Targeting regulated cell death in tumor nanomedicines. Theranostics 2022;12:817-41.
48. Sarter K, Leimgruber E, Gobet F, et al. Btn2a2, a T cell immunomodulatory molecule coregulated with MHC class II genes. J Exp Med 2016;213:177-87.
49. Vavassori S, Kumar A, Wan GS, et al. Butyrophilin 3A1 binds phosphorylated antigens and stimulates human γδ T cells. Nat Immunol 2013;14:908-16.
50. Neefjes J, Ovaa H. A peptide's perspective on antigen presentation to the immune system. Nat Chem Biol 2013;9:769-75.
51. Alspach E, Lussier DM, Miceli AP, et al. MHC-II neoantigens shape tumour immunity and response to immunotherapy. Nature 2019;574:696-701.
52. Axelrod ML, Cook RS, Johnson DB, et al. Biological Consequences of MHC-II Expression by Tumor Cells in Cancer. Clin Cancer Res 2019;25:2392-402.
53. Sha D, Jin Z, Budczies J, et al. Tumor Mutational Burden as a Predictive Biomarker in Solid Tumors. Cancer Discov 2020;10:1808-25.
54. Jardim DL, Goodman A, de Melo Gagliato D, et al. The Challenges of Tumor Mutational Burden as an Immunotherapy Biomarker. Cancer Cell 2021;39:154-73.

Cite this article as: Wang X, Jing H, Li H. A novel cuproptosis-related lncRNA signature to predict prognosis and immune landscape of lung adenocarcinoma. Transl Lung Cancer Res 2023;12(2):230-246. doi: 10.21037/tlcr-22-500

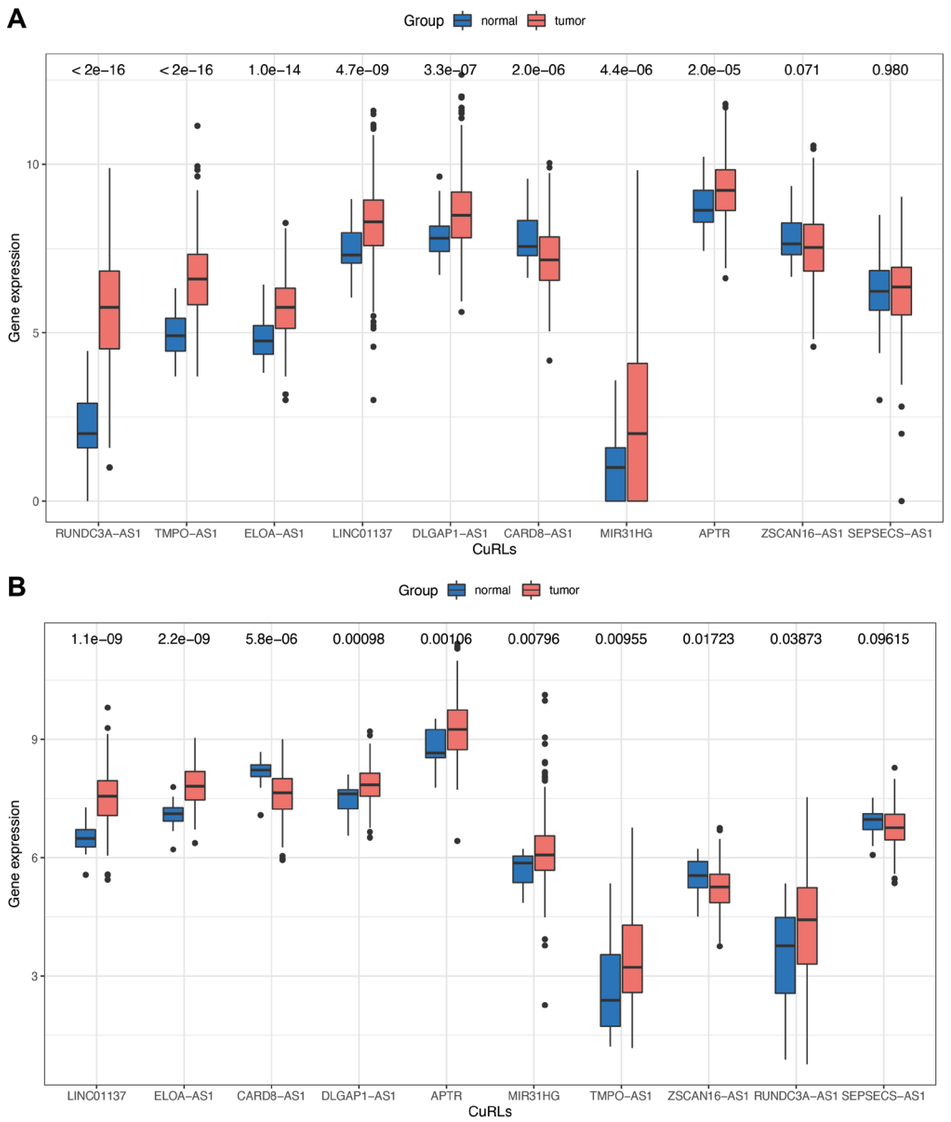

Figure S1 The differential expression of 10 CuRLs between normal and tumor tissues. (A) TCGA-LUAD cohort. (B) GSE31210. Abbreviations: CuRLs, cuproptosis-related lncRNAs.

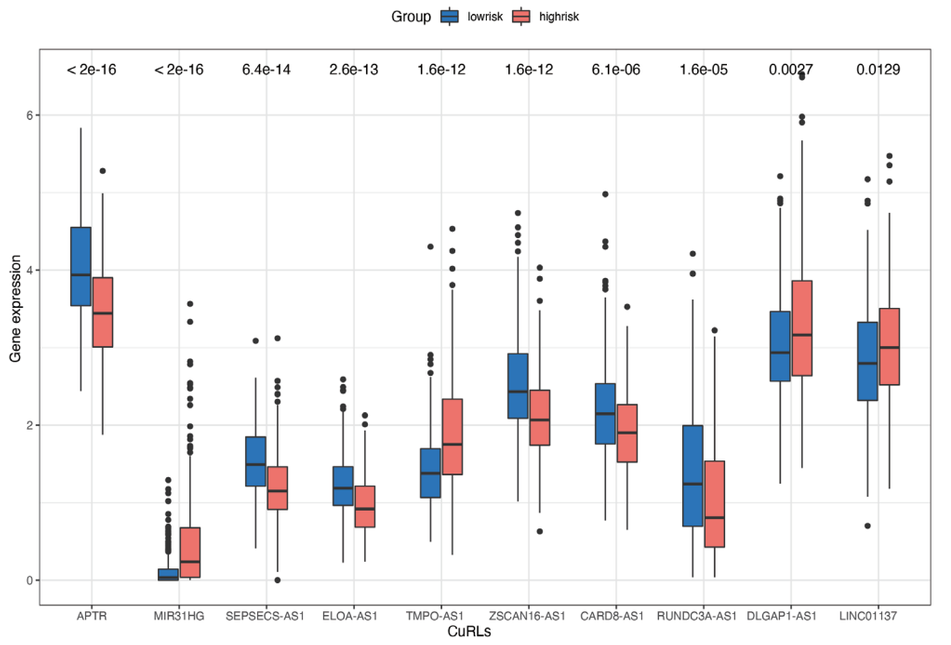

Figure S2 The differential expression of 10 CuRLs between low-risk and high-risk groups. CuRLs, cuproptosis-related lncRNAs.

https://dx.doi.org/10.21037/tlcr-22-500

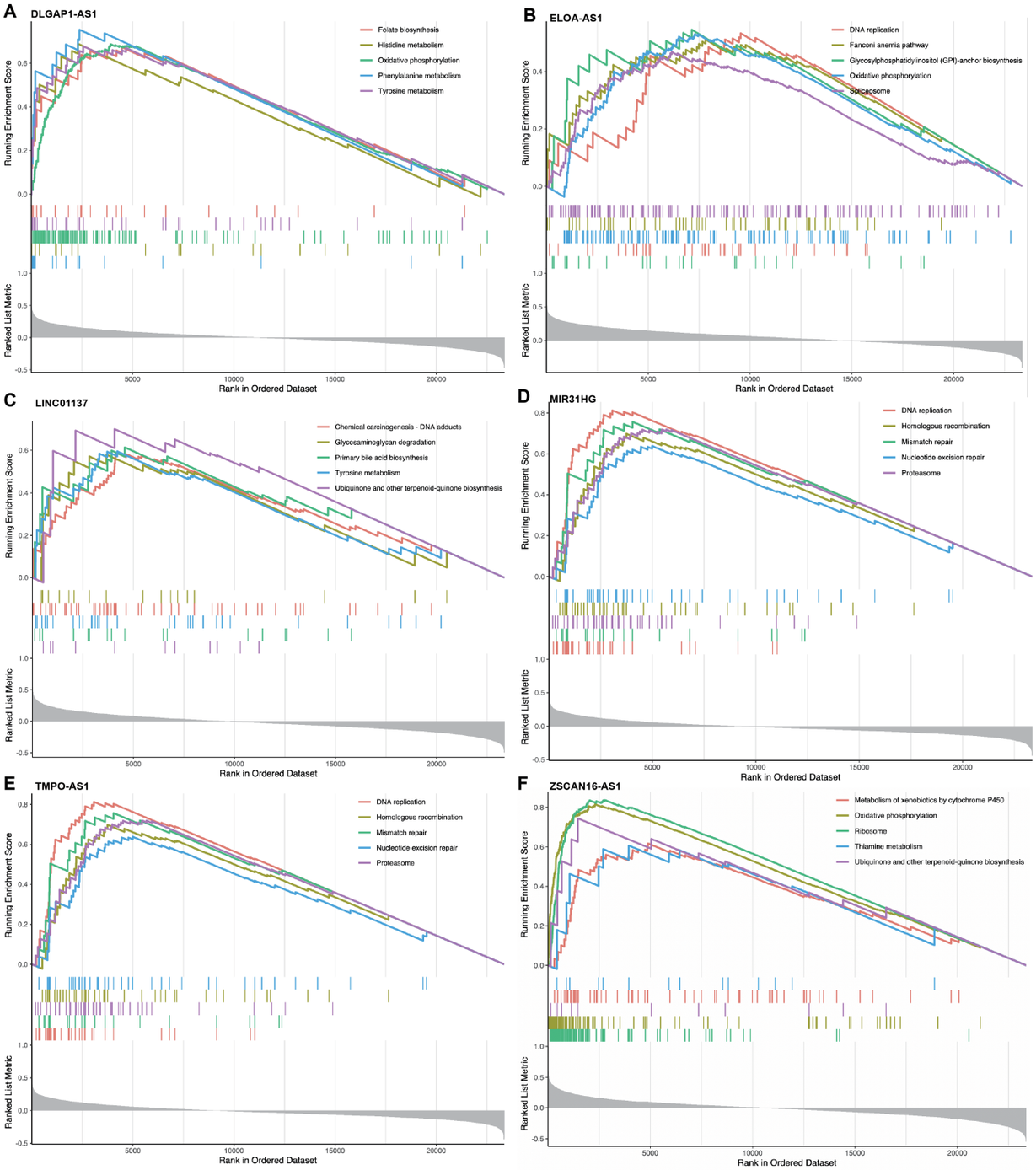

Figure S3 GSEA enrichment plots of CuRLs based on KEGG pathway database. (A) DLGAP1-AS1. (B) ELOA-AS1. (C) LINC01137. (D) MIR31HG. (E) TMPO-AS1. (F) ZSCAN16-AS1. CuRLs, cuproptosis-related lncRNAs; GSEA, gene set enrichment analysis; KEGG, Kyoto Encyclopedia of Genes and Genomes.

https://dx.doi.org/10.21037/tlcr-22-500

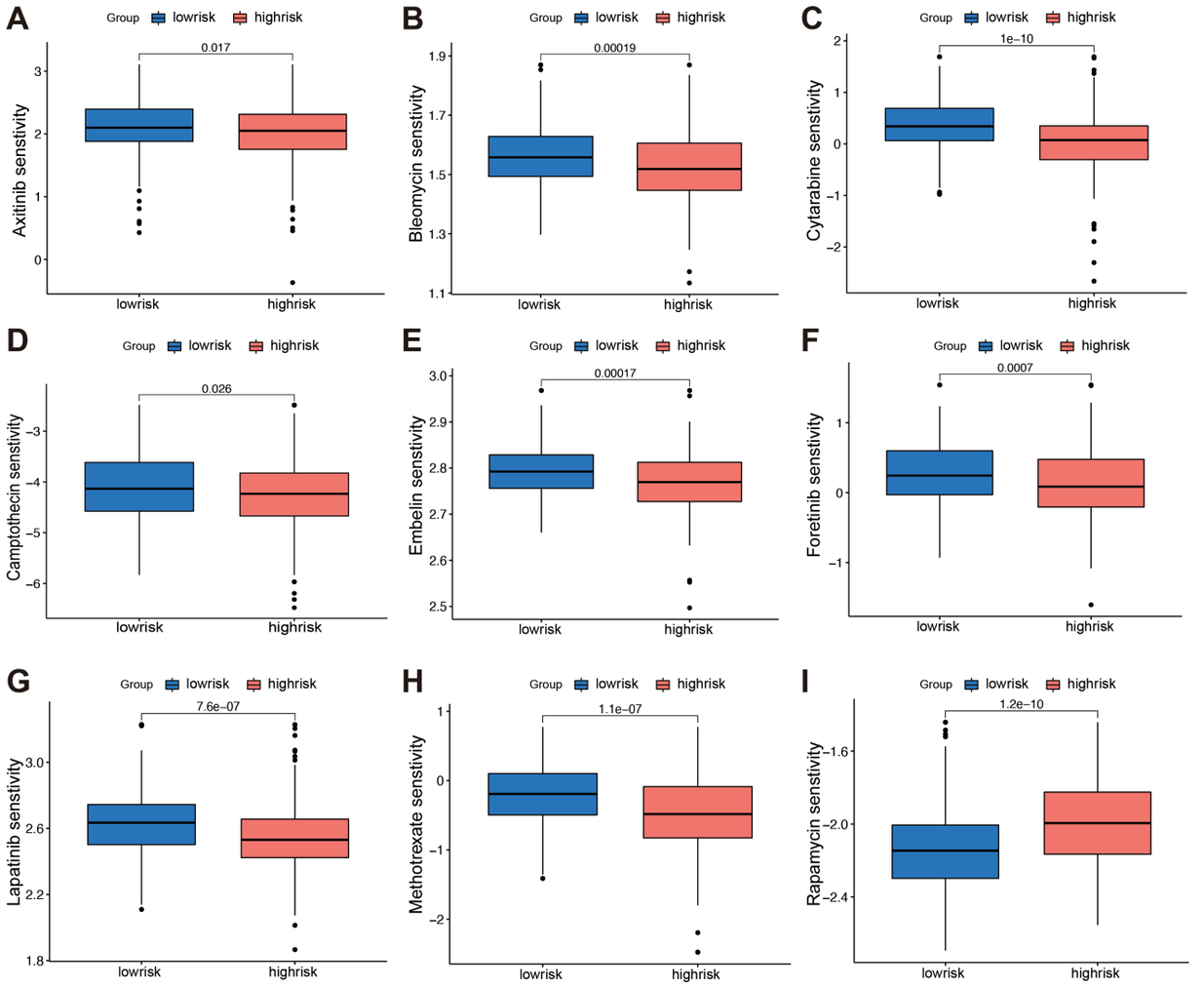

Figure S4 Predicted drug responses in low-risk and high-risk groups. (A) Axitinib, (B) Bleomycin, (C) Cytarabine, (D) Camptothecin, (E) Embelin, (F) Foretinib, (G) Lapatinib, (H) Methotrexate, (I) Rapamycin.

Table S1 Clinical characteristics of patients in training and validation datasets.

Characteristics	TCGA-LUAD (N=472)	GEO meta-cohort (N=458)
Gender (%)		
Male	217 (46.0)	215 (46.9)
Female	255 (54.0)	243 (53.1)
Age (%)		
≤65	209 (44.3)	273 (59.6)
>65	263 (55.7)	185 (40.4)
Stage (%)		
I	256 (54.2)	330 (72.1)
II	113 (23.9)	112 (24.5)
III	78 (16.5)	12 (2.6)
IV	25 (5.3)	4 (0.9)

GEO, Gene Expression Omnibus; LUAD, lung adenocarcinoma; TCGA, The Cancer Genome Atlas.

https://dx.doi.org/10.21037/tlcr-22-500

Table S2 Identified CuRLs using Pearson correlation analysis

	Cuproptosis genes	LncRNAs	Correlation coefficient	P value	Regulation
cor	MTF1	LINC01128	0.455	<0.001	Positive
cor1	LIPT2	LINC01770	0.309	<0.001	Positive
cor2	PDHB	TNFRSF14-AS1	−0.303	<0.001	Negative
cor3	DLAT	TNFRSF14-AS1	−0.385	<0.001	Negative
cor4	DLD	PRDM16-DT	−0.308	<0.001	Negative
cor5	LIPT2	LINC00337	0.333	<0.001	Positive
cor6	PDHB	TMEM51-AS1	−0.358	<0.001	Negative
cor7	MTF1	PINK1-AS	0.413	<0.001	Positive
cor8	LIPT1	LINC00339	0.411	<0.001	Positive
cor9	LIPT1	ELOA-AS1	0.313	<0.001	Positive
cor10	LIAS	LINC01137	0.31	<0.001	Positive
cor11	ATP7B	LINC01137	−0.31	<0.001	Negative
cor12	MTF1	SLFNL1-AS1	0.328	<0.001	Positive
cor13	MTF1	MKNK1-AS1	0.395	<0.001	Positive
cor14	MTF1	SSBP3-AS1	0.365	<0.001	Positive
cor15	DBT	LAMTOR5-AS1	0.307	<0.001	Positive
cor16	DBT	ATP1A1-AS1	0.402	<0.001	Positive
cor17	LIPT2	ZNF687-AS1	0.305	<0.001	Positive
cor18	PDHA1	RUSC1-AS1	0.31	<0.001	Positive
cor19	GLS	DNM3OS	0.305	<0.001	Positive
cor20	MTF1	GAS5	−0.466	<0.001	Negative
cor21	PDHB	GAS5	0.412	<0.001	Positive
cor22	LIAS	GAS5	0.357	<0.001	Positive
cor23	MTF1	SMG7-AS1	0.337	<0.001	Positive
cor24	LIPT2	LINC01136	0.333	<0.001	Positive
cor25	ATP7A	MIR29B2CHG	0.338	<0.001	Positive
cor26	LIAS	LINC00467	0.453	<0.001	Positive
cor27	LIPT2	LGALS8-AS1	0.348	<0.001	Positive
cor28	GCSH	RNASEH1-AS1	0.348	<0.001	Positive
cor29	LIPT2	ODC1-DT	0.301	<0.001	Positive
cor30	ATP7B	LINC00954	0.339	<0.001	Positive
cor31	FDX1	CRIM1-DT	0.328	<0.001	Positive
cor32	LIPT1	PCBP1-AS1	0.316	<0.001	Positive
cor33	LIPT2	LINC01816	0.451	<0.001	Positive
cor34	ATP7B	BOLA3-AS1	0.347	<0.001	Positive
cor35	ATP7B	LINC01943	−0.319	<0.001	Negative
cor36	LIPT2	EIF2AK3-DT	0.311	<0.001	Positive
cor37	GCSH	LINC00342	−0.322	<0.001	Negative
cor38	MTF1	STARD7-AS1	0.34	<0.001	Positive
cor39	LIPT1	NIFK-AS1	0.41	<0.001	Positive
cor40	GLS	HAGLR	0.315	<0.001	Positive
cor41	MTF1	CFLAR-AS1	0.304	<0.001	Positive
cor42	GLS	CFLAR-AS1	0.387	<0.001	Positive
cor43	ATP7A	CFLAR-AS1	0.304	<0.001	Positive
cor44	LIPT2	IDH1-AS1	0.351	<0.001	Positive
cor45	MTF1	LINC01963	0.451	<0.001	Positive
cor46	MTF1	CATIP-AS1	−0.337	<0.001	Negative
cor47	GLS	EGOT	0.327	<0.001	Positive

Table S2 *(continued)*

https://dx.doi.org/10.21037/tlcr-22-500

Table S2 *(continued)*

	Cuproptosis genes	LncRNAs	Correlation coefficient	P value	Regulation
cor48	GCSH	PRRT3-AS1	0.356	<0.001	Positive
cor49	DLD	SH3BP5-AS1	−0.302	<0.001	Negative
cor50	LIAS	EIF1B-AS1	0.395	<0.001	Positive
cor51	MTF1	ENTPD3-AS1	−0.308	<0.001	Negative
cor52	LIPT1	ENTPD3-AS1	0.313	<0.001	Positive
cor53	PDHB	ENTPD3-AS1	0.31	<0.001	Positive
cor54	LIAS	ENTPD3-AS1	0.415	<0.001	Positive
cor55	MTF1	PSMD6-AS2	0.342	<0.001	Positive
cor56	MTF1	LINC02035	0.513	<0.001	Positive
cor57	PDHB	LINC02035	−0.307	<0.001	Negative
cor58	GCSH	LINC02035	−0.313	<0.001	Negative
cor59	LIPT1	NCK1-DT	0.377	<0.001	Positive
cor60	LIPT2	WWTR1-AS1	0.34	<0.001	Positive
cor61	PDHA1	WWTR1-AS1	0.321	<0.001	Positive
cor62	GLS	LINC01214	0.369	<0.001	Positive
cor63	LIAS	TIPARP-AS1	0.307	<0.001	Positive
cor64	GLS	LINC00880	0.379	<0.001	Positive
cor65	GLS	LINC02029	0.342	<0.001	Positive
cor66	LIPT2	KCNMB2-AS1	0.323	<0.001	Positive
cor67	LIPT2	SOX2-OT	0.361	<0.001	Positive
cor68	LIPT2	LINC00884	0.33	<0.001	Positive
cor69	LIPT1	TMEM44-AS1	0.338	<0.001	Positive
cor70	LIPT2	TMEM44-AS1	0.392	<0.001	Positive
cor71	CDKN2A	MELTF-AS1	0.332	<0.001	Positive
cor72	PDHA1	MELTF-AS1	0.308	<0.001	Positive
cor73	LIAS	STX18-AS1	0.314	<0.001	Positive
cor74	LIPT2	LINC02482	0.324	<0.001	Positive
cor75	LIAS	LINC02481	0.33	<0.001	Positive
cor76	LIAS	TAPT1-AS1	0.351	<0.001	Positive
cor77	LIPT2	SEPSECS-AS1	0.305	<0.001	Positive
cor78	GLS	DANCR	−0.309	<0.001	Negative
cor79	LIPT2	DANCR	0.315	<0.001	Positive
cor80	GLS	LINC01094	0.35	<0.001	Positive
cor81	SLC31A1	LINC01094	0.335	<0.001	Positive
cor82	PDHA1	LINC01094	−0.348	<0.001	Negative
cor83	LIAS	WDFY3-AS2	0.357	<0.001	Positive
cor84	ATP7A	WDFY3-AS2	0.326	<0.001	Positive
cor85	LIAS	UBE2D3-AS1	0.38	<0.001	Positive
cor86	LIPT1	SEC24B-AS1	0.3	<0.001	Positive
cor87	MTF1	SNHG8	−0.374	<0.001	Negative
cor88	LIAS	SNHG8	0.404	<0.001	Positive
cor89	GLS	PART1	−0.302	<0.001	Negative
cor90	LIPT1	SCAMP1-AS1	0.404	<0.001	Positive
cor91	LIAS	SCAMP1-AS1	0.323	<0.001	Positive
cor92	LIAS	TMEM161B-AS1	0.314	<0.001	Positive
cor93	GLS	MEF2C-AS1	0.331	<0.001	Positive
cor94	GLS	NR2F1-AS1	0.307	<0.001	Positive

Table S2 *(continued)*

https://dx.doi.org/10.21037/tlcr-22-500

Table S2 *(continued)*

	Cuproptosis genes	LncRNAs	Correlation coefficient	P value	Regulation
cor95	PDHA1	NR2F1-AS1	−0.314	<0.001	Negative
cor96	DLD	RGMB-AS1	−0.319	<0.001	Negative
cor97	MTF1	LINC01023	−0.35	<0.001	Negative
cor98	DLAT	LINC01023	−0.307	<0.001	Negative
cor99	DLAT	IRF1-AS1	−0.305	<0.001	Negative
cor100	GCSH	IRF1-AS1	−0.316	<0.001	Negative
cor101	MTF1	TRIM52-AS1	−0.329	<0.001	Negative
cor102	MTF1	HCG11	0.384	<0.001	Positive
cor103	MTF1	ZSCAN16-AS1	−0.394	<0.001	Negative
cor104	GLS	HLA-F-AS1	0.383	<0.001	Positive
cor105	DBT	HCG18	0.329	<0.001	Positive
cor106	DLAT	HCG27	−0.301	<0.001	Negative
cor107	LIPT1	TRAM2-AS1	0.35	<0.001	Positive
cor108	LIAS	TRAM2-AS1	0.352	<0.001	Positive
cor109	GLS	WAKMAR2	0.336	<0.001	Positive
cor110	DBT	PRKAR1B-AS1	−0.301	<0.001	Negative
cor111	LIAS	SEPTIN7-DT	0.313	<0.001	Positive
cor112	ATP7A	SEPTIN7-DT	0.318	<0.001	Positive
cor113	MTF1	LINC00265	0.372	<0.001	Positive
cor114	PDHB	LINC00265	−0.339	<0.001	Negative
cor115	PDHB	POLR2J4	−0.312	<0.001	Negative
cor116	LIPT1	APTR	0.32	<0.001	Positive
cor117	PDHA1	MAGI2-AS3	−0.305	<0.001	Negative
cor118	DLD	EMSLR	0.342	<0.001	Positive
cor119	MTF1	PAXIP1-AS2	0.311	<0.001	Positive
cor120	ATP7A	PAXIP1-AS2	0.458	<0.001	Positive
cor121	GLS	LINC00689	−0.328	<0.001	Negative
cor122	MTF1	SNHG6	−0.389	<0.001	Negative
cor123	ATP7A	SNHG6	−0.347	<0.001	Negative
cor124	GLS	LACTB2-AS1	0.331	<0.001	Positive
cor125	LIPT2	STAU2-AS1	0.329	<0.001	Positive
cor126	MTF1	MINCR	−0.32	<0.001	Negative
cor127	LIAS	MINCR	0.307	<0.001	Positive
cor128	CDKN2A	MIR31HG	0.316	<0.001	Positive
cor129	CDKN2A	CDKN2B-AS1	0.645	<0.001	Positive
cor130	MTF1	GSN-AS1	0.377	<0.001	Positive
cor131	GCSH	GSN-AS1	−0.3	<0.001	Negative
cor132	ATP7B	SLC25A25-AS1	0.326	<0.001	Positive
cor133	DLAT	DBH-AS1	−0.32	<0.001	Negative
cor134	DLAT	NALT1	−0.317	<0.001	Negative
cor135	MTF1	CELF2-AS1	0.303	<0.001	Positive
cor136	ATP7A	CELF2-AS1	0.307	<0.001	Positive
cor137	LIPT2	DLG5-AS1	0.389	<0.001	Positive
cor138	MTF1	ENTPD1-AS1	0.342	<0.001	Positive
cor139	DBT	ENTPD1-AS1	0.353	<0.001	Positive
cor140	ATP7A	ENTPD1-AS1	0.345	<0.001	Positive
cor141	LIPT2	OLMALINC	0.345	<0.001	Positive

Table S2 *(continued)*

https://dx.doi.org/10.21037/tlcr-22-500

Table S2 *(continued)*

	Cuproptosis genes	LncRNAs	Correlation coefficient	P value	Regulation
cor142	DLD	LMNTD2-AS1	−0.304	<0.001	Negative
cor143	LIPT2	LINC02749	0.347	<0.001	Positive
cor144	LIPT2	LINC02709	0.337	<0.001	Positive
cor145	LIPT2	SBF2-AS1	0.307	<0.001	Positive
cor146	MTF1	MALAT1	0.312	<0.001	Positive
cor147	LIPT2	RAB30-DT	0.408	<0.001	Positive
cor148	LIPT2	LINC02762	0.323	<0.001	Positive
cor149	GCSH	GSEC	0.325	<0.001	Positive
cor150	LIPT1	ZBTB44-DT	0.303	<0.001	Positive
cor151	LIAS	ZBTB44-DT	0.349	<0.001	Positive
cor152	LIPT2	LOH12CR2	0.315	<0.001	Positive
cor153	GLS	RASSF8-AS1	0.357	<0.001	Positive
cor154	CDKN2A	DDX11-AS1	0.309	<0.001	Positive
cor155	LIPT2	LINC02387	0.333	<0.001	Positive
cor156	ATP7B	LINC02387	0.345	<0.001	Positive
cor157	LIPT2	ADCY6-DT	0.413	<0.001	Positive
cor158	FDX1	LINC00592	0.348	<0.001	Positive
cor159	PDHA1	AGAP2-AS1	−0.306	<0.001	Negative
cor160	LIPT2	LINC01465	0.328	<0.001	Positive
cor161	LIPT2	TMPO-AS1	0.437	<0.001	Positive
cor162	PDHA1	TMPO-AS1	0.353	<0.001	Positive
cor163	DLD	FAM222A-AS1	0.315	<0.001	Positive
cor164	MTF1	MAPKAPK5-AS1	−0.454	<0.001	Negative
cor165	LIPT1	MAPKAPK5-AS1	0.35	<0.001	Positive
cor166	LIAS	MAPKAPK5-AS1	0.347	<0.001	Positive
cor167	LIPT2	MAPKAPK5-AS1	0.349	<0.001	Positive
cor168	GCSH	MAPKAPK5-AS1	0.356	<0.001	Positive
cor169	GCSH	TBX5-AS1	−0.317	<0.001	Negative
cor170	PDHA1	TBX5-AS1	−0.321	<0.001	Negative
cor171	MTF1	PXN-AS1	−0.392	<0.001	Negative
cor172	LIAS	PXN-AS1	0.366	<0.001	Positive
cor173	LIPT2	PXN-AS1	0.326	<0.001	Positive
cor174	LIPT2	NRAV	0.301	<0.001	Positive
cor175	GLS	LINC00944	0.324	<0.001	Positive
cor176	ATP7B	TUSC8	0.312	<0.001	Positive
cor177	PDHB	DLEU1	0.328	<0.001	Positive
cor178	LIAS	DLEU1	0.328	<0.001	Positive
cor179	ATP7B	SOX21-AS1	0.378	<0.001	Positive
cor180	MTF1	LINC00641	0.365	<0.001	Positive
cor181	DLST	DHRS4-AS1	0.347	<0.001	Positive
cor182	GLS	NKX2-1-AS1	0.303	<0.001	Positive
cor183	LIPT2	FOXN3-AS1	0.303	<0.001	Positive
cor184	DLAT	DIO3OS	−0.302	<0.001	Negative
cor185	ATP7A	LINC02256	0.302	<0.001	Positive
cor186	GLS	LINC02345	0.333	<0.001	Positive
cor187	GLS	LINC01852	0.347	<0.001	Positive
cor188	GLS	SPINT1-AS1	−0.312	<0.001	Negative

Table S2 *(continued)*

https://dx.doi.org/10.21037/tlcr-22-500

Table S2 *(continued)*

	Cuproptosis genes	LncRNAs	Correlation coefficient	P value	Regulation
cor189	DBT	OIP5-AS1	0.338	<0.001	Positive
cor190	LIAS	EIF3J-DT	0.338	<0.001	Positive
cor191	LIPT2	IQCH-AS1	0.318	<0.001	Positive
cor192	LIPT2	DRAIC	0.36	<0.001	Positive
cor193	MTF1	NPTN-IT1	0.425	<0.001	Positive
cor194	LIPT2	UBL7-AS1	0.357	<0.001	Positive
cor195	LIPT2	TMC3-AS1	0.312	<0.001	Positive
cor196	MTF1	ZNF710-AS1	0.314	<0.001	Positive
cor197	MTF1	SNHG9	−0.338	<0.001	Negative
cor198	GLS	LINC02861	0.311	<0.001	Positive
cor199	GCSH	VPS9D1-AS1	0.301	<0.001	Positive
cor200	MTF1	PITPNA-AS1	−0.37	<0.001	Negative
cor201	LIPT2	PITPNA-AS1	0.403	<0.001	Positive
cor202	GCSH	PITPNA-AS1	0.337	<0.001	Positive
cor203	DLAT	MIR497HG	−0.333	<0.001	Negative
cor204	MTF1	SNHG29	−0.39	<0.001	Negative
cor205	PDHB	SNHG29	0.454	<0.001	Positive
cor206	MTF1	LINC02693	0.435	<0.001	Positive
cor207	ATP7B	RAMP2-AS1	0.314	<0.001	Positive
cor208	GLS	RUNDC3A-AS1	0.357	<0.001	Positive
cor209	LIPT2	TOB1-AS1	0.363	<0.001	Positive
cor210	GLS	LINC02003	0.362	<0.001	Positive
cor211	DLAT	SNHG16	0.327	<0.001	Positive
cor212	MTF1	RNF213-AS1	0.363	<0.001	Positive
cor213	DLD	BAIAP2-DT	−0.336	<0.001	Negative
cor214	LIPT2	TYMSOS	0.312	<0.001	Positive
cor215	MTF1	GAPLINC	−0.369	<0.001	Negative
cor216	GLS	DLGAP1-AS1	−0.36	<0.001	Negative
cor217	LIPT2	DLGAP1-AS1	0.302	<0.001	Positive
cor218	LIPT2	LINC00668	0.336	<0.001	Positive
cor219	DLAT	GATA6-AS1	−0.336	<0.001	Negative
cor220	PDHA1	CARD8-AS1	−0.365	<0.001	Negative
cor221	MTF1	PTOV1-AS1	0.311	<0.001	Positive
cor222	LIPT2	NRSN2-AS1	0.313	<0.001	Positive
cor223	LIPT2	LINC01431	0.33	<0.001	Positive
cor224	MTF1	NORAD	0.467	<0.001	Positive
cor225	DBT	NORAD	0.302	<0.001	Positive
cor226	ATP7A	NORAD	0.354	<0.001	Positive
cor227	ATP7A	SNHG17	−0.35	<0.001	Negative
cor228	LIPT2	SNHG11	0.353	<0.001	Positive
cor229	LIPT1	OSER1-DT	0.398	<0.001	Positive
cor230	MTF1	ZFAS1	−0.444	<0.001	Negative
cor231	ATP7A	ZFAS1	−0.314	<0.001	Negative
cor232	LIPT1	URB1-AS1	0.304	<0.001	Positive
cor233	GCSH	URB1-AS1	0.307	<0.001	Positive
cor234	LIPT1	C21orf62-AS1	0.324	<0.001	Positive
cor235	ATP7A	C21orf62-AS1	0.328	<0.001	Positive

Table S2 *(continued)*

https://dx.doi.org/10.21037/tlcr-22-500

Table S2 *(continued)*

	Cuproptosis genes	LncRNAs	Correlation coefficient	P value	Regulation
cor236	GLS	IL10RB-DT	0.314	<0.001	Positive
cor237	ATP7B	B3GALT5-AS1	0.331	<0.001	Positive
cor238	LIPT2	TRPM2-AS	0.353	<0.001	Positive
cor239	DLAT	ITGB2-AS1	−0.33	<0.001	Negative
cor240	ATP7B	LINC01547	−0.312	<0.001	Negative
cor241	MTF1	MCM3AP-AS1	0.337	<0.001	Positive
cor242	LIPT2	THAP7-AS1	0.304	<0.001	Positive
cor243	MTF1	PPM1F-AS1	0.333	<0.001	Positive
cor244	PDHB	PPM1F-AS1	−0.321	<0.001	Negative
cor245	MTF1	LINC01521	0.318	<0.001	Positive
cor246	MTF1	PRR34-AS1	−0.316	<0.001	Negative
cor247	DLAT	LINC00685	−0.314	<0.001	Negative
cor248	SLC31A1	ASMTL-AS1	−0.305	<0.001	Negative
cor249	PDHA1	ASMTL-AS1	0.32	<0.001	Positive
cor250	PDHA1	ZNF674-AS1	0.355	<0.001	Positive
cor251	ATP7A	LINC01278	0.378	<0.001	Positive
cor252	ATP7A	FTX	0.475	<0.001	Positive
cor253	ATP7A	RAP2C-AS1	0.439	<0.001	Positive

CuRLs, cuproptosis-related lncRNAs.

https://dx.doi.org/10.21037/tlcr-22-500

Table S3 Univariate Cox regression analysis of CuRLs associated with OS of LUAD

LncRNAs	HR (95% CI)	P value	Risk type
LINC00592	1.671 (1.258, 2.221)	<0.001	Risk
TMPO-AS1	1.443 (1.185, 1.758)	<0.001	Risk
GSEC	1.401 (1.197, 1.640)	<0.001	Risk
NKX2-1-AS1	0.814 (0.726, 0.911)	<0.001	Protect
APTR	0.701 (0.567, 0.867)	0.001	Protect
MIR31HG	1.414 (1.139, 1.757)	0.002	Risk
PRDM16-DT	0.809 (0.701, 0.934)	0.004	Protect
PCBP1-AS1	0.662 (0.498, 0.879)	0.004	Protect
MIR497HG	0.537 (0.352, 0.820)	0.004	Protect
MIR4435-2HG	1.315 (1.088, 1.590)	0.005	Risk
ZNF674-AS1	0.695 (0.535, 0.902)	0.006	Protect
LINC01137	1.304 (1.074, 1.583)	0.007	Risk
MIR29B2CHG	0.845 (0.747, 0.956)	0.007	Protect
TBX5-AS1	0.796 (0.675, 0.938)	0.007	Protect
NIFK-AS1	0.599 (0.414, 0.867)	0.007	Protect
ZSCAN16-AS1	0.734 (0.580, 0.929)	0.010	Protect
ELOA-AS1	0.607 (0.415, 0.886)	0.010	Protect
DLGAP1-AS1	1.239 (1.051, 1.459)	0.011	Risk
IRF1-AS1	0.765 (0.619, 0.944)	0.013	Protect
LINC01852	0.618 (0.423, 0.904)	0.013	Protect
LINC02709	1.442 (1.074, 1.938)	0.015	Risk
ZNF710-AS1	0.802 (0.672, 0.958)	0.015	Protect
CARD8-AS1	0.747 (0.585, 0.954)	0.019	Protect
SEPSECS-AS1	0.702 (0.518, 0.951)	0.023	Protect
HCG18	0.693 (0.497, 0.966)	0.031	Protect
HAGLR	0.913 (0.841, 0.992)	0.032	Protect
BAIAP2-DT	0.842 (0.719, 0.986)	0.032	Protect
TYMSOS	1.309 (1.021, 1.677)	0.033	Risk
DDX11-AS1	1.409 (1.026, 1.936)	0.034	Risk
LINC02861	0.788 (0.632, 0.983)	0.035	Protect
IL10RB-DT	0.720 (0.530, 0.977)	0.035	Protect
CRIM1-DT	1.317 (1.015, 1.707)	0.038	Risk
DRAIC	0.912 (0.837, 0.995)	0.038	Protect
SCAMP1-AS1	0.759 (0.584, 0.985)	0.038	Protect
RUNDC3A-AS1	0.813 (0.669, 0.989)	0.039	Protect
PSMD6-AS2	0.687 (0.477, 0.990)	0.044	Protect

CI, confidence interval; CuRLs, cuproptosis-related lncRNAs; HR,hazard ratio; LUAD, lung adenocarcinoma; OS, overall survival.

https://dx.doi.org/10.21037/tlcr-22-500

Table S4 Identified CuRLs-related mRNAs using Pearson correlation analysis

CuRLs	mRNA	Correlation coefficient	P value	Regulation
CARD8-AS1	TNFRSF9	0.528	<0.001	Positive
LINC01137	AGTRAP	0.541	<0.001	Positive
CARD8-AS1	NECAP2	0.620	<0.001	Positive
CARD8-AS1	PLA2G5	0.525	<0.001	Positive
CARD8-AS1	PLA2G2D	0.509	<0.001	Positive
CARD8-AS1	C1QA	0.607	<0.001	Positive
CARD8-AS1	C1QC	0.618	<0.001	Positive
CARD8-AS1	C1QB	0.615	<0.001	Positive
TMPO-AS1	E2F2	0.651	<0.001	Positive
ELOA-AS1	MTFR1L	0.524	<0.001	Positive
TMPO-AS1	AUNIP	0.587	<0.001	Positive
TMPO-AS1	STMN1	0.551	<0.001	Positive
CARD8-AS1	CD52	0.685	<0.001	Positive
CARD8-AS1	FGR	0.561	<0.001	Positive
CARD8-AS1	PTAFR	0.503	<0.001	Positive
ZSCAN16-AS1	ATP5IF1	0.544	<0.001	Positive
CARD8-AS1	LAPTM5	0.690	<0.001	Positive
ELOA-AS1	IQCC	0.518	<0.001	Positive
CARD8-AS1	LCK	0.618	<0.001	Positive
TMPO-AS1	CLSPN	0.598	<0.001	Positive
TMPO-AS1	CDCA8	0.639	<0.001	Positive
TMPO-AS1	CDC20	0.618	<0.001	Positive
TMPO-AS1	KIF2C	0.648	<0.001	Positive
TMPO-AS1	RAD54L	0.684	<0.001	Positive
TMPO-AS1	STIL	0.603	<0.001	Positive
TMPO-AS1	ORC1	0.631	<0.001	Positive
TMPO-AS1	DEPDC1	0.602	<0.001	Positive
CARD8-AS1	MCOLN2	0.563	<0.001	Positive
CARD8-AS1	GBP1	0.522	<0.001	Positive
CARD8-AS1	GBP4	0.519	<0.001	Positive
CARD8-AS1	GBP5	0.525	<0.001	Positive
CARD8-AS1	LRRC8C	0.568	<0.001	Positive
TMPO-AS1	CDC7	0.614	<0.001	Positive
CARD8-AS1	GFI1	0.503	<0.001	Positive
CARD8-AS1	VCAM1	0.503	<0.001	Positive
TMPO-AS1	PSRC1	0.624	<0.001	Positive
CARD8-AS1	CD53	0.760	<0.001	Positive
CARD8-AS1	C1orf162	0.599	<0.001	Positive
CARD8-AS1	TMIGD3	0.543	<0.001	Positive
CARD8-AS1	PTPN22	0.604	<0.001	Positive
CARD8-AS1	CD2	0.649	<0.001	Positive
CARD8-AS1	FCGR1B	0.641	<0.001	Positive
TMPO-AS1	FAM72B	0.638	<0.001	Positive
TMPO-AS1	FAM72C	0.567	<0.001	Positive
TMPO-AS1	FAM72D	0.618	<0.001	Positive
CARD8-AS1	FCGR1A	0.651	<0.001	Positive
CARD8-AS1	PLEKHO1	0.540	<0.001	Positive
CARD8-AS1	C1orf54	0.667	<0.001	Positive
CARD8-AS1	CTSS	0.605	<0.001	Positive
CARD8-AS1	CTSK	0.516	<0.001	Positive
CARD8-AS1	TNFAIP8L2	0.701	<0.001	Positive

Table S4 *(continued)*

https://dx.doi.org/10.21037/tlcr-22-500

Table S4 *(continued)*

CuRLs	mRNA	Correlation coefficient	P value	Regulation
ZSCAN16-AS1	DPM3	0.572	<0.001	Positive
CARD8-AS1	SYT11	0.504	<0.001	Positive
TMPO-AS1	IQGAP3	0.559	<0.001	Positive
CARD8-AS1	CD1D	0.634	<0.001	Positive
CARD8-AS1	MNDA	0.682	<0.001	Positive
CARD8-AS1	PYHIN1	0.590	<0.001	Positive
CARD8-AS1	SLAMF8	0.626	<0.001	Positive
CARD8-AS1	SLAMF6	0.604	<0.001	Positive
CARD8-AS1	CD84	0.638	<0.001	Positive
CARD8-AS1	SLAMF1	0.645	<0.001	Positive
CARD8-AS1	CD48	0.755	<0.001	Positive
CARD8-AS1	SLAMF7	0.615	<0.001	Positive
CARD8-AS1	LY9	0.537	<0.001	Positive
CARD8-AS1	CD244	0.628	<0.001	Positive
CARD8-AS1	ARHGAP30	0.533	<0.001	Positive
CARD8-AS1	FCER1G	0.645	<0.001	Positive
CARD8-AS1	FCGR2A	0.542	<0.001	Positive
CARD8-AS1	FCGR3A	0.607	<0.001	Positive
CARD8-AS1	FCGR2B	0.653	<0.001	Positive
CARD8-AS1	FCRLA	0.501	<0.001	Positive
TMPO-AS1	NUF2	0.617	<0.001	Positive
CARD8-AS1	CD247	0.612	<0.001	Positive
CARD8-AS1	RCSD1	0.675	<0.001	Positive
CARD8-AS1	XCL2	0.510	<0.001	Positive
TMPO-AS1	C1orf112	0.520	<0.001	Positive
CARD8-AS1	SELL	0.541	<0.001	Positive
CARD8-AS1	FMO2	0.500	<0.001	Positive
TMPO-AS1	CENPL	0.508	<0.001	Positive
CARD8-AS1	NPL	0.592	<0.001	Positive
CARD8-AS1	NCF2	0.575	<0.001	Positive
CARD8-AS1	RGS18	0.772	<0.001	Positive
CARD8-AS1	RGS13	0.578	<0.001	Positive
TMPO-AS1	ASPM	0.615	<0.001	Positive
CARD8-AS1	PTPRC	0.722	<0.001	Positive
TMPO-AS1	KIF14	0.620	<0.001	Positive
CARD8-AS1	PTPN7	0.612	<0.001	Positive
TMPO-AS1	UBE2T	0.574	<0.001	Positive
CARD8-AS1	LAX1	0.534	<0.001	Positive
TMPO-AS1	FAM72A	0.646	<0.001	Positive
CARD8-AS1	IL10	0.692	<0.001	Positive
CARD8-AS1	FCMR	0.549	<0.001	Positive
TMPO-AS1	C1orf116	-0.538	<0.001	Negative
CARD8-AS1	CR1	0.585	<0.001	Positive
CARD8-AS1	HSD11B1	0.662	<0.001	Positive
CARD8-AS1	TRAF3IP3	0.611	<0.001	Positive
TMPO-AS1	NEK2	0.611	<0.001	Positive
TMPO-AS1	DTL	0.604	<0.001	Positive
TMPO-AS1	CENPF	0.602	<0.001	Positive
CARD8-AS1	KMO	0.558	<0.001	Positive
TMPO-AS1	EXO1	0.647	<0.001	Positive
CARD8-AS1	NLRP3	0.534	<0.001	Positive

Table S4 *(continued)*

https://dx.doi.org/10.21037/tlcr-22-500

Table S4 *(continued)*

CuRLs	mRNA	Correlation coefficient	P value	Regulation
TMPO-AS1	RRM2	0.617	<0.001	Positive
CARD8-AS1	CYRIA	0.524	<0.001	Positive
TMPO-AS1	GEN1	0.567	<0.001	Positive
TMPO-AS1	CENPO	0.602	<0.001	Positive
TMPO-AS1	CENPA	0.648	<0.001	Positive
CARD8-AS1	NLRC4	0.604	<0.001	Positive
CARD8-AS1	RASGRP3	0.500	<0.001	Positive
ZSCAN16-AS1	ACYP2	0.512	<0.001	Positive
CARD8-AS1	CNRIP1	0.557	<0.001	Positive
CARD8-AS1	PLEK	0.714	<0.001	Positive
CARD8-AS1	ARHGAP25	0.607	<0.001	Positive
ZSCAN16-AS1	PRADC1	0.507	<0.001	Positive
CARD8-AS1	CD8A	0.531	<0.001	Positive
CARD8-AS1	CD8B	0.512	<0.001	Positive
TMPO-AS1	NCAPH	0.650	<0.001	Positive
CARD8-AS1	IL18RAP	0.517	<0.001	Positive
TMPO-AS1	BUB1	0.626	<0.001	Positive
TMPO-AS1	CKAP2L	0.610	<0.001	Positive
CARD8-AS1	GYPC	0.605	<0.001	Positive
TMPO-AS1	MCM6	0.571	<0.001	Positive
CARD8-AS1	CXCR4	0.522	<0.001	Positive
CARD8-AS1	ARHGAP15	0.736	<0.001	Positive
CARD8-AS1	ZEB2	0.611	<0.001	Positive
CARD8-AS1	CYTIP	0.596	<0.001	Positive
TMPO-AS1	SPC25	0.687	<0.001	Positive
CARD8-AS1	WIPF1	0.608	<0.001	Positive
CARD8-AS1	ITGA4	0.601	<0.001	Positive
CARD8-AS1	CALCRL	0.503	<0.001	Positive
TMPO-AS1	CCDC150	0.537	<0.001	Positive
CARD8-AS1	ANKRD44	0.522	<0.001	Positive
TMPO-AS1	SGO2	0.567	<0.001	Positive
CARD8-AS1	CD28	0.645	<0.001	Positive
CARD8-AS1	CTLA4	0.509	<0.001	Positive
CARD8-AS1	ICOS	0.659	<0.001	Positive
CARD8-AS1	ARPC2	0.504	<0.001	Positive
TMPO-AS1	CNOT9	0.502	<0.001	Positive
CARD8-AS1	DOCK10	0.529	<0.001	Positive
CARD8-AS1	SP140	0.527	<0.001	Positive
TMPO-AS1	HJURP	0.648	<0.001	Positive
ZSCAN16-AS1	COPS9	0.522	<0.001	Positive
TMPO-AS1	FANCD2	0.590	<0.001	Positive
CARD8-AS1	ATG7	0.503	<0.001	Positive
TMPO-AS1	SGO1	0.641	<0.001	Positive
CARD8-AS1	EOMES	0.505	<0.001	Positive
CARD8-AS1	CCR4	0.583	<0.001	Positive
CARD8-AS1	CCR8	0.509	<0.001	Positive
TMPO-AS1	KIF15	0.626	<0.001	Positive
CARD8-AS1	CXCR6	0.605	<0.001	Positive
CARD8-AS1	CCR1	0.625	<0.001	Positive
CARD8-AS1	CCR2	0.700	<0.001	Positive
CARD8-AS1	CCR5	0.613	<0.001	Positive

Table S4 *(continued)*

https://dx.doi.org/10.21037/tlcr-22-500

Table S4 *(continued)*

CuRLs	mRNA	Correlation coefficient	P value	Regulation
CARD8-AS1	CCRL2	0.510	<0.001	Positive
TMPO-AS1	CDC25A	0.644	<0.001	Positive
ZSCAN16-AS1	TMA7	0.503	<0.001	Positive
TMPO-AS1	TRAIP	0.589	<0.001	Positive
TMPO-AS1	POC1A	0.527	<0.001	Positive
CARD8-AS1	PPM1M	0.538	<0.001	Positive
ZSCAN16-AS1	SMIM4	0.520	<0.001	Positive
CARD8-AS1	KBTBD8	0.734	<0.001	Positive
TMPO-AS1	CIP2A	0.607	<0.001	Positive
CARD8-AS1	TRAT1	0.646	<0.001	Positive
CARD8-AS1	CD96	0.565	<0.001	Positive
CARD8-AS1	CD200	0.525	<0.001	Positive
CARD8-AS1	BTLA	0.622	<0.001	Positive
CARD8-AS1	CD200R1	0.699	<0.001	Positive
CARD8-AS1	CD80	0.666	<0.001	Positive
TMPO-AS1	POLQ	0.662	<0.001	Positive
CARD8-AS1	CD86	0.722	<0.001	Positive
TMPO-AS1	MCM2	0.625	<0.001	Positive
TMPO-AS1	TOPBP1	0.585	<0.001	Positive
CARD8-AS1	SLC9A9	0.591	<0.001	Positive
CARD8-AS1	P2RY14	0.618	<0.001	Positive
CARD8-AS1	P2RY13	0.679	<0.001	Positive
CARD8-AS1	P2RY12	0.649	<0.001	Positive
CARD8-AS1	SUCNR1	0.511	<0.001	Positive
TMPO-AS1	GMPS	0.554	<0.001	Positive
CARD8-AS1	LXN	0.522	<0.001	Positive
CARD8-AS1	MFSD1	0.509	<0.001	Positive
TMPO-AS1	ECT2	0.546	<0.001	Positive
CARD8-AS1	GNB4	0.501	<0.001	Positive
CARD8-AS1	KLHL6	0.577	<0.001	Positive
TMPO-AS1	TRA2B	0.500	<0.001	Positive
TMPO-AS1	RFC4	0.645	<0.001	Positive
CARD8-AS1	NRROS	0.513	<0.001	Positive
TMPO-AS1	TACC3	0.611	<0.001	Positive
TMPO-AS1	NSD2	0.512	<0.001	Positive
CARD8-AS1	SLC2A9	0.567	<0.001	Positive
CARD8-AS1	BST1	0.530	<0.001	Positive
CARD8-AS1	LAP3	0.518	<0.001	Positive
TMPO-AS1	NCAPG	0.645	<0.001	Positive
CARD8-AS1	TLR10	0.598	<0.001	Positive
CARD8-AS1	TLR1	0.584	<0.001	Positive
CARD8-AS1	RHOH	0.545	<0.001	Positive
TMPO-AS1	HOPX	-0.542	<0.001	Negative
CARD8-AS1	IGFBP7	0.511	<0.001	Positive
CARD8-AS1	STAP1	0.573	<0.001	Positive
CARD8-AS1	JCHAIN	0.534	<0.001	Positive
CARD8-AS1	CXCL10	0.549	<0.001	Positive
CARD8-AS1	CXCL13	0.529	<0.001	Positive
TMPO-AS1	H2AZ1	0.536	<0.001	Positive
TMPO-AS1	CENPE	0.612	<0.001	Positive
CARD8-AS1	MCUB	0.501	<0.001	Positive

Table S4 *(continued)*

https://dx.doi.org/10.21037/tlcr-22-500

Table S4 *(continued)*

CuRLs	mRNA	Correlation coefficient	P value	Regulation
TMPO-AS1	MAD2L1	0.547	<0.001	Positive
TMPO-AS1	CCNA2	0.598	<0.001	Positive
TMPO-AS1	PLK4	0.610	<0.001	Positive
CARD8-AS1	IL15	0.515	<0.001	Positive
TMPO-AS1	MND1	0.540	<0.001	Positive
CARD8-AS1	MARCHF1	0.738	<0.001	Positive
TMPO-AS1	HMGB2	0.564	<0.001	Positive
TMPO-AS1	CENPU	0.588	<0.001	Positive
TMPO-AS1	TRIP13	0.532	<0.001	Positive
CARD8-AS1	IL7R	0.595	<0.001	Positive
TMPO-AS1	SKP2	0.520	<0.001	Positive
CARD8-AS1	SLC1A3	0.566	<0.001	Positive
CARD8-AS1	FYB1	0.593	<0.001	Positive
CARD8-AS1	PTGER4	0.577	<0.001	Positive
TMPO-AS1	C5orf34	0.544	<0.001	Positive
CARD8-AS1	GZMK	0.629	<0.001	Positive
CARD8-AS1	GZMA	0.569	<0.001	Positive
CARD8-AS1	GAPT	0.613	<0.001	Positive
TMPO-AS1	DEPDC1B	0.578	<0.001	Positive
TMPO-AS1	CENPK	0.581	<0.001	Positive
CARD8-AS1	SGTB	0.545	<0.001	Positive
CARD8-AS1	CD180	0.662	<0.001	Positive
TMPO-AS1	CCNB1	0.596	<0.001	Positive
TMPO-AS1	CENPH	0.610	<0.001	Positive
CARD8-AS1	NAIP	0.595	<0.001	Positive
CARD8-AS1	CAMK4	0.526	<0.001	Positive
CARD8-AS1	TNFAIP8	0.577	<0.001	Positive
TMPO-AS1	LMNB1	0.634	<0.001	Positive
CARD8-AS1	TIFAB	0.606	<0.001	Positive
TMPO-AS1	KIF20A	0.615	<0.001	Positive
TMPO-AS1	CDC25C	0.638	<0.001	Positive
CARD8-AS1	CD14	0.565	<0.001	Positive
ZSCAN16-AS1	NDUFA2	0.596	<0.001	Positive
CARD8-AS1	CSF1R	0.569	<0.001	Positive
CARD8-AS1	CDX1	0.520	<0.001	Positive
CARD8-AS1	HAVCR2	0.699	<0.001	Positive
CARD8-AS1	ITK	0.577	<0.001	Positive
TMPO-AS1	PTTG1	0.544	<0.001	Positive
TMPO-AS1	HMMR	0.585	<0.001	Positive
CARD8-AS1	MAT2B	0.516	<0.001	Positive
TMPO-AS1	SPDL1	0.538	<0.001	Positive
CARD8-AS1	DOCK2	0.608	<0.001	Positive
CARD8-AS1	LCP2	0.680	<0.001	Positive
CARD8-AS1	HK3	0.506	<0.001	Positive
CARD8-AS1	LY86	0.676	<0.001	Positive
TMPO-AS1	GMNN	0.534	<0.001	Positive
CARD8-AS1	BTN3A1	0.512	<0.001	Positive
CARD8-AS1	BTN3A3	0.512	<0.001	Positive
TMPO-AS1	TCF19	0.579	<0.001	Positive
CARD8-AS1	LTA	0.589	<0.001	Positive
CARD8-AS1	LST1	0.706	<0.001	Positive

Table S4 *(continued)*

https://dx.doi.org/10.21037/tlcr-22-500

Table S4 *(continued)*

CuRLs	mRNA	Correlation coefficient	P value	Regulation
CARD8-AS1	NCR3	0.589	<0.001	Positive
CARD8-AS1	AIF1	0.721	<0.001	Positive
CARD8-AS1	HLA-DRA	0.641	<0.001	Positive
CARD8-AS1	HLA-DRB1	0.514	<0.001	Positive
CARD8-AS1	HLA-DQA1	0.583	<0.001	Positive
CARD8-AS1	HLA-DOB	0.512	<0.001	Positive
CARD8-AS1	PSMB9	0.502	<0.001	Positive
CARD8-AS1	HLA-DMB	0.670	<0.001	Positive
CARD8-AS1	AL645941.2	0.522	<0.001	Positive
CARD8-AS1	HLA-DOA	0.536	<0.001	Positive
CARD8-AS1	HLA-DPA1	0.567	<0.001	Positive
CARD8-AS1	HLA-DPB1	0.562	<0.001	Positive
TMPO-AS1	KIFC1	0.671	<0.001	Positive
ZSCAN16-AS1	CUTA	0.580	<0.001	Positive
CARD8-AS1	FGD2	0.616	<0.001	Positive
CARD8-AS1	TREM2	0.553	<0.001	Positive
CARD8-AS1	TDRD6	0.512	<0.001	Positive
CARD8-AS1	PLA2G7	0.508	<0.001	Positive
TMPO-AS1	MCM3	0.554	<0.001	Positive
TMPO-AS1	TTK	0.640	<0.001	Positive
CARD8-AS1	CYB5R4	0.532	<0.001	Positive
TMPO-AS1	MMS22L	0.532	<0.001	Positive
CARD8-AS1	OSTM1	0.617	<0.001	Positive
CARD8-AS1	SNX3	0.501	<0.001	Positive
CARD8-AS1	DSE	0.511	<0.001	Positive
CARD8-AS1	CALHM6	0.612	<0.001	Positive
TMPO-AS1	CENPW	0.615	<0.001	Positive
CARD8-AS1	THEMIS	0.673	<0.001	Positive
CARD8-AS1	ARHGAP18	0.589	<0.001	Positive
CARD8-AS1	SAMD3	0.648	<0.001	Positive
CARD8-AS1	VNN2	0.583	<0.001	Positive
TMPO-AS1	MTFR2	0.598	<0.001	Positive
CARD8-AS1	IFNGR1	0.524	<0.001	Positive
CARD8-AS1	STX11	0.604	<0.001	Positive
CARD8-AS1	RAB32	0.558	<0.001	Positive
TMPO-AS1	FBXO5	0.610	<0.001	Positive
CARD8-AS1	TAGAP	0.680	<0.001	Positive
CARD8-AS1	CCR6	0.508	<0.001	Positive
CARD8-AS1	GPNMB	0.506	<0.001	Positive
CARD8-AS1	SNX10	0.547	<0.001	Positive
CARD8-AS1	CPVL	0.576	<0.001	Positive
TMPO-AS1	ANLN	0.535	<0.001	Positive
CARD8-AS1	AOAH	0.690	<0.001	Positive
CARD8-AS1	GPR141	0.579	<0.001	Positive
CARD8-AS1	IKZF1	0.617	<0.001	Positive
CARD8-AS1	LAT2	0.626	<0.001	Positive
CARD8-AS1	NCF1	0.617	<0.001	Positive
CARD8-AS1	FGL2	0.694	<0.001	Positive
APTR	RSBN1L	0.581	<0.001	Positive
TMPO-AS1	MCM7	0.518	<0.001	Positive
ZSCAN16-AS1	LAMTOR4	0.509	<0.001	Positive

Table S4 *(continued)*

https://dx.doi.org/10.21037/tlcr-22-500

Table S4 *(continued)*

CuRLs	mRNA	Correlation coefficient	P value	Regulation
CARD8-AS1	PILRA	0.610	<0.001	Positive
CARD8-AS1	PIK3CG	0.664	<0.001	Positive
CARD8-AS1	TFEC	0.775	<0.001	Positive
CARD8-AS1	CPED1	0.588	<0.001	Positive
ZSCAN16-AS1	FMC1	0.580	<0.001	Positive
CARD8-AS1	TPK1	0.514	<0.001	Positive
TMPO-AS1	EZH2	0.600	<0.001	Positive
CARD8-AS1	GIMAP8	0.518	<0.001	Positive
CARD8-AS1	GIMAP7	0.690	<0.001	Positive
CARD8-AS1	GIMAP4	0.721	<0.001	Positive
CARD8-AS1	GIMAP6	0.709	<0.001	Positive
CARD8-AS1	GIMAP2	0.690	<0.001	Positive
CARD8-AS1	GIMAP1	0.544	<0.001	Positive
CARD8-AS1	GIMAP5	0.597	<0.001	Positive
TMPO-AS1	XRCC2	0.556	<0.001	Positive
TMPO-AS1	NCAPG2	0.595	<0.001	Positive
CARD8-AS1	MSR1	0.628	<0.001	Positive
CARD8-AS1	ATP6V1B2	0.523	<0.001	Positive
CARD8-AS1	DOK2	0.637	<0.001	Positive
CARD8-AS1	ADAMDEC1	0.507	<0.001	Positive
TMPO-AS1	CDCA2	0.661	<0.001	Positive
TMPO-AS1	ESCO2	0.620	<0.001	Positive
TMPO-AS1	PBK	0.638	<0.001	Positive
TMPO-AS1	GINS4	0.552	<0.001	Positive
TMPO-AS1	MCM4	0.569	<0.001	Positive
CARD8-AS1	DNAJC5B	0.623	<0.001	Positive
CARD8-AS1	LY96	0.501	<0.001	Positive
CARD8-AS1	IL7	0.503	<0.001	Positive
TMPO-AS1	RAD54B	0.550	<0.001	Positive
TMPO-AS1	CCNE2	0.514	<0.001	Positive
TMPO-AS1	FBXO43	0.535	<0.001	Positive
TMPO-AS1	DSCC1	0.555	<0.001	Positive
TMPO-AS1	TBC1D31	0.518	<0.001	Positive
TMPO-AS1	ATAD2	0.543	<0.001	Positive
CARD8-AS1	SLA	0.623	<0.001	Positive
CARD8-AS1	FAM83H	-0.524	<0.001	Negative
CARD8-AS1	DOCK8	0.531	<0.001	Positive
CARD8-AS1	JAK2	0.600	<0.001	Positive
CARD8-AS1	PDCD1LG2	0.700	<0.001	Positive
MIR31HG	IFNE	0.774	<0.001	Positive
CARD8-AS1	C9orf72	0.502	<0.001	Positive
TMPO-AS1	KIF24	0.516	<0.001	Positive
CARD8-AS1	CCL19	0.543	<0.001	Positive
TMPO-AS1	FANCG	0.580	<0.001	Positive
CARD8-AS1	CD72	0.597	<0.001	Positive
CARD8-AS1	SIT1	0.678	<0.001	Positive
TMPO-AS1	ARHGEF39	0.661	<0.001	Positive
CARD8-AS1	GLIPR2	0.626	<0.001	Positive
TMPO-AS1	MELK	0.612	<0.001	Positive
CARD8-AS1	SUSD3	0.555	<0.001	Positive
TMPO-AS1	ZNF367	0.613	<0.001	Positive

Table S4 *(continued)*

https://dx.doi.org/10.21037/tlcr-22-500

Table S4 *(continued)*

CuRLs	mRNA	Correlation coefficient	P value	Regulation
TMPO-AS1	SMC2	0.519	<0.001	Positive
CARD8-AS1	SLC31A2	0.652	<0.001	Positive
CARD8-AS1	TNFSF8	0.675	<0.001	Positive
CARD8-AS1	TLR4	0.729	<0.001	Positive
CARD8-AS1	FAM78A	0.552	<0.001	Positive
CARD8-AS1	FCN1	0.507	<0.001	Positive
CARD8-AS1	IL2RA	0.559	<0.001	Positive
TMPO-AS1	MCM10	0.585	<0.001	Positive
CARD8-AS1	APBB1IP	0.546	<0.001	Positive
TMPO-AS1	MASTL	0.571	<0.001	Positive
CARD8-AS1	TMEM273	0.774	<0.001	Positive
TMPO-AS1	ZWINT	0.679	<0.001	Positive
TMPO-AS1	CDK1	0.607	<0.001	Positive
TMPO-AS1	DNA2	0.561	<0.001	Positive
CARD8-AS1	SRGN	0.630	<0.001	Positive
TMPO-AS1	DNAJC9	0.520	<0.001	Positive
CARD8-AS1	LIPA	0.571	<0.001	Positive
TMPO-AS1	KIF20B	0.524	<0.001	Positive
TMPO-AS1	KIF11	0.658	<0.001	Positive
TMPO-AS1	CEP55	0.574	<0.001	Positive
TMPO-AS1	HELLS	0.651	<0.001	Positive
CARD8-AS1	ENTPD1	0.616	<0.001	Positive
CARD8-AS1	PIK3AP1	0.681	<0.001	Positive
CARD8-AS1	CALHM2	0.510	<0.001	Positive
ZSCAN16-AS1	SLK	-0.522	<0.001	Negative
TMPO-AS1	MKI67	0.615	<0.001	Positive
CARD8-AS1	TRIM22	0.524	<0.001	Positive
TMPO-AS1	E2F8	0.572	<0.001	Positive
TMPO-AS1	CCDC34	0.543	<0.001	Positive
TMPO-AS1	KIF18A	0.551	<0.001	Positive
CARD8-AS1	SPI1	0.574	<0.001	Positive
ZSCAN16-AS1	CTNND1	-0.509	<0.001	Negative
CARD8-AS1	LPXN	0.691	<0.001	Positive
TMPO-AS1	FAM111B	0.574	<0.001	Positive
CARD8-AS1	MPEG1	0.638	<0.001	Positive
CARD8-AS1	MS4A6A	0.748	<0.001	Positive
CARD8-AS1	MS4A4A	0.683	<0.001	Positive
CARD8-AS1	MS4A7	0.630	<0.001	Positive
TMPO-AS1	FEN1	0.638	<0.001	Positive
TMPO-AS1	INCENP	0.566	<0.001	Positive
CARD8-AS1	FERMT3	0.630	<0.001	Positive
CARD8-AS1	NAALADL1	0.622	<0.001	Positive
TMPO-AS1	CDCA5	0.654	<0.001	Positive
TMPO-AS1	POLA2	0.649	<0.001	Positive
TMPO-AS1	CNIH2	0.503	<0.001	Positive
LINC01137	RHOD	0.501	<0.001	Positive
ZSCAN16-AS1	KDM2A	-0.511	<0.001	Negative
CARD8-AS1	TBC1D10C	0.567	<0.001	Positive
TMPO-AS1	TESMIN	0.571	<0.001	Positive
CARD8-AS1	FOLR2	0.609	<0.001	Positive
CARD8-AS1	SLCO2B1	0.588	<0.001	Positive

Table S4 *(continued)*

https://dx.doi.org/10.21037/tlcr-22-500

Table S4 *(continued)*

CuRLs	mRNA	Correlation coefficient	P value	Regulation
TMPO-AS1	DDIAS	0.561	<0.001	Positive
CARD8-AS1	CASP5	0.503	<0.001	Positive
CARD8-AS1	CASP1	0.643	<0.001	Positive
CARD8-AS1	CARD16	0.553	<0.001	Positive
CARD8-AS1	IL10RA	0.659	<0.001	Positive
CARD8-AS1	JAML	0.599	<0.001	Positive
CARD8-AS1	CD3E	0.557	<0.001	Positive
CARD8-AS1	CD3D	0.618	<0.001	Positive
CARD8-AS1	CD3G	0.611	<0.001	Positive
ZSCAN16-AS1	BCL9L	-0.544	<0.001	Negative
TMPO-AS1	H2AX	0.513	<0.001	Positive
CARD8-AS1	CRTAM	0.642	<0.001	Positive
CARD8-AS1	SLC37A2	0.542	<0.001	Positive
TMPO-AS1	CHEK1	0.650	<0.001	Positive
TMPO-AS1	ACRV1	0.589	<0.001	Positive
TMPO-AS1	HYLS1	0.501	<0.001	Positive
CARD8-AS1	FLI1	0.580	<0.001	Positive
TMPO-AS1	NCAPD3	0.514	<0.001	Positive
TMPO-AS1	FOXM1	0.664	<0.001	Positive
TMPO-AS1	RAD51AP1	0.614	<0.001	Positive
CARD8-AS1	CD27	0.516	<0.001	Positive
TMPO-AS1	NCAPD2	0.568	<0.001	Positive
CARD8-AS1	CD4	0.631	<0.001	Positive
TMPO-AS1	CDCA3	0.686	<0.001	Positive
CARD8-AS1	CD163	0.537	<0.001	Positive
CARD8-AS1	C3AR1	0.651	<0.001	Positive
CARD8-AS1	CLEC4A	0.776	<0.001	Positive
CARD8-AS1	CLEC6A	0.619	<0.001	Positive
CARD8-AS1	CLEC4D	0.526	<0.001	Positive
CARD8-AS1	KLRG1	0.595	<0.001	Positive
CARD8-AS1	KLRB1	0.628	<0.001	Positive
CARD8-AS1	CLECL1	0.662	<0.001	Positive
CARD8-AS1	CD69	0.671	<0.001	Positive
CARD8-AS1	CLEC2B	0.526	<0.001	Positive
CARD8-AS1	CLEC12A	0.587	<0.001	Positive
CARD8-AS1	CLEC7A	0.563	<0.001	Positive
TMPO-AS1	GPR19	0.600	<0.001	Positive
CARD8-AS1	PTPRO	0.675	<0.001	Positive
CARD8-AS1	LRMP	0.587	<0.001	Positive
CARD8-AS1	ABCD2	0.637	<0.001	Positive
TMPO-AS1	SENP1	0.527	<0.001	Positive
TMPO-AS1	TUBA1B	0.501	<0.001	Positive
TMPO-AS1	TROAP	0.706	<0.001	Positive
TMPO-AS1	SPATS2	0.540	<0.001	Positive
CARD8-AS1	FMNL3	0.502	<0.001	Positive
TMPO-AS1	RACGAP1	0.666	<0.001	Positive
CARD8-AS1	BIN2	0.609	<0.001	Positive
CARD8-AS1	ITGB7	0.556	<0.001	Positive
TMPO-AS1	ESPL1	0.698	<0.001	Positive
ZSCAN16-AS1	PFDN5	0.537	<0.001	Positive
CARD8-AS1	NCKAP1L	0.673	<0.001	Positive

Table S4 *(continued)*

https://dx.doi.org/10.21037/tlcr-22-500

Table S4 *(continued)*

CuRLs	mRNA	Correlation coefficient	P value	Regulation
CARD8-AS1	TESPA1	0.573	<0.001	Positive
TMPO-AS1	CDK2	0.659	<0.001	Positive
TMPO-AS1	PA2G4	0.507	<0.001	Positive
TMPO-AS1	TIMELESS	0.665	<0.001	Positive
TMPO-AS1	PRIM1	0.602	<0.001	Positive
TMPO-AS1	NEMP1	0.543	<0.001	Positive
CARD8-AS1	ARHGAP9	0.596	<0.001	Positive
TMPO-AS1	NUP107	0.511	<0.001	Positive
CARD8-AS1	LYZ	0.606	<0.001	Positive
CARD8-AS1	GLIPR1	0.672	<0.001	Positive
TMPO-AS1	E2F7	0.636	<0.001	Positive
CARD8-AS1	LUM	0.520	<0.001	Positive
CARD8-AS1	DCN	0.576	<0.001	Positive
CARD8-AS1	PLXNC1	0.634	<0.001	Positive
TMPO-AS1	SNRPF	0.569	<0.001	Positive
TMPO-AS1	TMPO	0.705	<0.001	Positive
TMPO-AS1	NUP37	0.534	<0.001	Positive
TMPO-AS1	PARPBP	0.619	<0.001	Positive
TMPO-AS1	TDG	0.560	<0.001	Positive
CARD8-AS1	CMKLR1	0.602	<0.001	Positive
CARD8-AS1	SELPLG	0.607	<0.001	Positive
TMPO-AS1	UNG	0.610	<0.001	Positive
TMPO-AS1	ANAPC7	0.563	<0.001	Positive
CARD8-AS1	HVCN1	0.579	<0.001	Positive
TMPO-AS1	RFC5	0.691	<0.001	Positive
TMPO-AS1	SRSF9	0.527	<0.001	Positive
TMPO-AS1	C12orf43	0.517	<0.001	Positive
CARD8-AS1	P2RX7	0.600	<0.001	Positive
ZSCAN16-AS1	CLIP1	-0.502	<0.001	Negative
TMPO-AS1	KNTC1	0.656	<0.001	Positive
TMPO-AS1	DENR	0.518	<0.001	Positive
TMPO-AS1	KMT5A	0.509	<0.001	Positive
TMPO-AS1	DDX55	0.557	<0.001	Positive
TMPO-AS1	EIF2B1	0.513	<0.001	Positive
TMPO-AS1	BRI3BP	0.573	<0.001	Positive
TMPO-AS1	POLE	0.606	<0.001	Positive
TMPO-AS1	SKA3	0.649	<0.001	Positive
CARD8-AS1	MTMR6	0.511	<0.001	Positive
CARD8-AS1	FLT3	0.511	<0.001	Positive
CARD8-AS1	ALOX5AP	0.566	<0.001	Positive
TMPO-AS1	BRCA2	0.550	<0.001	Positive
CARD8-AS1	N4BP2L1	0.561	<0.001	Positive
TMPO-AS1	RFC3	0.571	<0.001	Positive
CARD8-AS1	EPSTI1	0.508	<0.001	Positive
CARD8-AS1	LCP1	0.629	<0.001	Positive
CARD8-AS1	RUBCNL	0.603	<0.001	Positive
CARD8-AS1	LPAR6	0.640	<0.001	Positive
CARD8-AS1	RCBTB2	0.572	<0.001	Positive
CARD8-AS1	CYSLTR2	0.521	<0.001	Positive
TMPO-AS1	CKAP2	0.535	<0.001	Positive
TMPO-AS1	DIAPH3	0.557	<0.001	Positive

Table S4 *(continued)*

https://dx.doi.org/10.21037/tlcr-22-500

Table S4 *(continued)*

CuRLs	mRNA	Correlation coefficient	P value	Regulation
TMPO-AS1	BORA	0.534	<0.001	Positive
CARD8-AS1	GPR18	0.625	<0.001	Positive
CARD8-AS1	GPR183	0.565	<0.001	Positive
CARD8-AS1	TNFSF13B	0.732	<0.001	Positive
CARD8-AS1	RNASE6	0.701	<0.001	Positive
CARD8-AS1	SLC7A7	0.660	<0.001	Positive
TMPO-AS1	POLE2	0.606	<0.001	Positive
CARD8-AS1	GNG2	0.637	<0.001	Positive
TMPO-AS1	CDKN3	0.595	<0.001	Positive
TMPO-AS1	WDHD1	0.520	<0.001	Positive
TMPO-AS1	DLGAP5	0.625	<0.001	Positive
CARD8-AS1	RTN1	0.530	<0.001	Positive
RUNDC3A-AS1	TMEM63C	0.511	<0.001	Positive
CARD8-AS1	GPR65	0.807	<0.001	Positive
ZSCAN16-AS1	NDUFB1	0.577	<0.001	Positive
ZSCAN16-AS1	GON7	0.522	<0.001	Positive
CARD8-AS1	ASB2	0.549	<0.001	Positive
TMPO-AS1	VRK1	0.548	<0.001	Positive
TMPO-AS1	ARHGAP11A	0.655	<0.001	Positive
TMPO-AS1	BUB1B	0.671	<0.001	Positive
TMPO-AS1	KNSTRN	0.588	<0.001	Positive
TMPO-AS1	KNL1	0.662	<0.001	Positive
TMPO-AS1	RAD51	0.617	<0.001	Positive
TMPO-AS1	OIP5	0.677	<0.001	Positive
TMPO-AS1	NUSAP1	0.697	<0.001	Positive
TMPO-AS1	WDR76	0.620	<0.001	Positive
CARD8-AS1	B2M	0.663	<0.001	Positive
TMPO-AS1	CEP152	0.518	<0.001	Positive
CARD8-AS1	ATP8B4	0.611	<0.001	Positive
CARD8-AS1	LYSMD2	0.529	<0.001	Positive
TMPO-AS1	CCNB2	0.647	<0.001	Positive
CARD8-AS1	LACTB	0.528	<0.001	Positive
CARD8-AS1	RAB8B	0.637	<0.001	Positive
TMPO-AS1	PCLAF	0.604	<0.001	Positive
TMPO-AS1	PIF1	0.634	<0.001	Positive
CARD8-AS1	PLEKHO2	0.667	<0.001	Positive
TMPO-AS1	TIPIN	0.540	<0.001	Positive
TMPO-AS1	ZWILCH	0.594	<0.001	Positive
TMPO-AS1	KIF23	0.674	<0.001	Positive
CARD8-AS1	PSTPIP1	0.570	<0.001	Positive
CARD8-AS1	BCL2A1	0.662	<0.001	Positive
CARD8-AS1	IL16	0.659	<0.001	Positive
CARD8-AS1	TM6SF1	0.634	<0.001	Positive
TMPO-AS1	FANCI	0.735	<0.001	Positive
TMPO-AS1	TICRR	0.709	<0.001	Positive
TMPO-AS1	BLM	0.667	<0.001	Positive
TMPO-AS1	RCCD1	0.544	<0.001	Positive
TMPO-AS1	PRC1	0.719	<0.001	Positive
TMPO-AS1	SNRPA1	0.596	<0.001	Positive
TMPO-AS1	CCNF	0.513	<0.001	Positive
TMPO-AS1	TEDC2	0.556	<0.001	Positive

Table S4 *(continued)*

https://dx.doi.org/10.21037/tlcr-22-500

Table S4 *(continued)*

CuRLs	mRNA	Correlation coefficient	P value	Regulation
TMPO-AS1	PKMYT1	0.585	<0.001	Positive
TMPO-AS1	C16orf89	-0.501	<0.001	Negative
TMPO-AS1	RMI2	0.527	<0.001	Positive
CARD8-AS1	TNFRSF17	0.505	<0.001	Positive
ZSCAN16-AS1	ITPRIPL2	-0.504	<0.001	Negative
TMPO-AS1	REXO5	0.533	<0.001	Positive
CARD8-AS1	IGSF6	0.730	<0.001	Positive
TMPO-AS1	PLK1	0.642	<0.001	Positive
CARD8-AS1	PRKCB	0.553	<0.001	Positive
CARD8-AS1	IL21R	0.586	<0.001	Positive
CARD8-AS1	SPN	0.544	<0.001	Positive
CARD8-AS1	C16orf54	0.545	<0.001	Positive
TMPO-AS1	KIF22	0.507	<0.001	Positive
CARD8-AS1	CORO1A	0.564	<0.001	Positive
CARD8-AS1	ITGAL	0.548	<0.001	Positive
CARD8-AS1	ZNF267	0.519	<0.001	Positive
TMPO-AS1	SHCBP1	0.525	<0.001	Positive
TMPO-AS1	ORC6	0.629	<0.001	Positive
CARD8-AS1	SNX20	0.629	<0.001	Positive
TMPO-AS1	GINS3	0.529	<0.001	Positive
CARD8-AS1	DPEP2	0.565	<0.001	Positive
CARD8-AS1	MAF	0.509	<0.001	Positive
TMPO-AS1	CENPN	0.581	<0.001	Positive
CARD8-AS1	COTL1	0.502	<0.001	Positive
TMPO-AS1	GINS2	0.593	<0.001	Positive
CARD8-AS1	IRF8	0.726	<0.001	Positive
TMPO-AS1	CDT1	0.640	<0.001	Positive
TMPO-AS1	FANCA	0.616	<0.001	Positive
TMPO-AS1	HASPIN	0.613	<0.001	Positive
CARD8-AS1	PELP1	-0.536	<0.001	Negative
CARD8-AS1	SCIMP	0.698	<0.001	Positive
TMPO-AS1	PIMREG	0.606	<0.001	Positive
CARD8-AS1	CLEC10A	0.669	<0.001	Positive
CARD8-AS1	ACAP1	0.501	<0.001	Positive
TMPO-AS1	AURKB	0.615	<0.001	Positive
CARD8-AS1	PIK3R5	0.557	<0.001	Positive
CARD8-AS1	PMP22	0.520	<0.001	Positive
CARD8-AS1	TRPV2	0.598	<0.001	Positive
TMPO-AS1	SPAG5	0.661	<0.001	Positive
ZSCAN16-AS1	NUFIP2	-0.519	<0.001	Negative
TMPO-AS1	ATAD5	0.565	<0.001	Positive
CARD8-AS1	ADAP2	0.509	<0.001	Positive
CARD8-AS1	EVI2B	0.717	<0.001	Positive
CARD8-AS1	EVI2A	0.833	<0.001	Positive
CARD8-AS1	SLFN12L	0.505	<0.001	Positive
CARD8-AS1	CCL5	0.510	<0.001	Positive
TMPO-AS1	RDM1	0.551	<0.001	Positive
CARD8-AS1	CCL23	0.516	<0.001	Positive
CARD8-AS1	CCL3	0.546	<0.001	Positive
CARD8-AS1	CCL4	0.559	<0.001	Positive
TMPO-AS1	CDC6	0.610	<0.001	Positive

Table S4 *(continued)*

https://dx.doi.org/10.21037/tlcr-22-500

Table S4 *(continued)*

CuRLs	mRNA	Correlation coefficient	P value	Regulation
TMPO-AS1	TOP2A	0.595	<0.001	Positive
TMPO-AS1	PSMC3IP	0.581	<0.001	Positive
TMPO-AS1	BRCA1	0.595	<0.001	Positive
TMPO-AS1	HROB	0.568	<0.001	Positive
TMPO-AS1	DBF4B	0.576	<0.001	Positive
TMPO-AS1	KIF18B	0.681	<0.001	Positive
CARD8-AS1	GNGT2	0.631	<0.001	Positive
CARD8-AS1	ABI3	0.648	<0.001	Positive
TMPO-AS1	EME1	0.591	<0.001	Positive
TMPO-AS1	PRR11	0.577	<0.001	Positive
TMPO-AS1	BRIP1	0.564	<0.001	Positive
CARD8-AS1	CD79B	0.596	<0.001	Positive
CARD8-AS1	MILR1	0.521	<0.001	Positive
TMPO-AS1	KPNA2	0.516	<0.001	Positive
CARD8-AS1	ABCA6	0.534	<0.001	Positive
CARD8-AS1	CD300A	0.665	<0.001	Positive
CARD8-AS1	CD300C	0.604	<0.001	Positive
CARD8-AS1	CD300LF	0.653	<0.001	Positive
TMPO-AS1	TK1	0.503	<0.001	Positive
TMPO-AS1	BIRC5	0.606	<0.001	Positive
TMPO-AS1	TYMS	0.609	<0.001	Positive
TMPO-AS1	NDC80	0.656	<0.001	Positive
DLGAP1-AS1	TGIF1	0.635	<0.001	Positive
TMPO-AS1	SKA1	0.658	<0.001	Positive
TMPO-AS1	C18orf54	0.508	<0.001	Positive
CARD8-AS1	CD226	0.623	<0.001	Positive
CARD8-AS1	EBI3	0.513	<0.001	Positive
TMPO-AS1	CHAF1A	0.549	<0.001	Positive
TMPO-AS1	UHRF1	0.556	<0.001	Positive
ZSCAN16-AS1	PET100	0.504	<0.001	Positive
CARD8-AS1	MYO1F	0.540	<0.001	Positive
CARD8-AS1	ICAM3	0.656	<0.001	Positive
CARD8-AS1	C19orf38	0.522	<0.001	Positive
TMPO-AS1	SPC24	0.645	<0.001	Positive
TMPO-AS1	RNASEH2A	0.545	<0.001	Positive
CARD8-AS1	LYL1	0.502	<0.001	Positive
TMPO-AS1	ASF1B	0.626	<0.001	Positive
CARD8-AS1	CLEC17A	0.537	<0.001	Positive
CARD8-AS1	IL12RB1	0.599	<0.001	Positive
CARD8-AS1	LRRC25	0.611	<0.001	Positive
CARD8-AS1	ZNF101	0.540	<0.001	Positive
TMPO-AS1	CCNE1	0.514	<0.001	Positive
TMPO-AS1	FAAP24	0.514	<0.001	Positive
CARD8-AS1	HCST	0.592	<0.001	Positive
CARD8-AS1	TYROBP	0.654	<0.001	Positive
TMPO-AS1	WDR62	0.511	<0.001	Positive
CARD8-AS1	MAP4K1	0.515	<0.001	Positive
CARD8-AS1	GMFG	0.771	<0.001	Positive
CARD8-AS1	CEACAM21	0.580	<0.001	Positive
CARD8-AS1	APOC1	0.534	<0.001	Positive
CARD8-AS1	PLA2G4C	0.521	<0.001	Positive

Table S4 *(continued)*

https://dx.doi.org/10.21037/tlcr-22-500

Table S4 *(continued)*

CuRLs	mRNA	Correlation coefficient	P value	Regulation
TMPO-AS1	LIG1	0.506	<0.001	Positive
CARD8-AS1	EMP3	0.533	<0.001	Positive
CARD8-AS1	CD37	0.583	<0.001	Positive
TMPO-AS1	NAPSA	-0.530	<0.001	Negative
CARD8-AS1	SIGLEC9	0.611	<0.001	Positive
CARD8-AS1	SIGLEC7	0.654	<0.001	Positive
CARD8-AS1	CD33	0.665	<0.001	Positive
CARD8-AS1	SIGLEC10	0.582	<0.001	Positive
CARD8-AS1	SIGLEC14	0.529	<0.001	Positive
CARD8-AS1	FPR1	0.591	<0.001	Positive
CARD8-AS1	FPR3	0.640	<0.001	Positive
CARD8-AS1	OSCAR	0.503	<0.001	Positive
CARD8-AS1	LILRB2	0.573	<0.001	Positive
CARD8-AS1	LILRA5	0.594	<0.001	Positive
CARD8-AS1	LILRA4	0.568	<0.001	Positive
CARD8-AS1	LAIR1	0.656	<0.001	Positive
CARD8-AS1	LILRA1	0.561	<0.001	Positive
CARD8-AS1	LILRB1	0.616	<0.001	Positive
CARD8-AS1	LILRB4	0.567	<0.001	Positive
CARD8-AS1	TMEM150B	0.549	<0.001	Positive
TMPO-AS1	UBE2S	0.549	<0.001	Positive
CARD8-AS1	SIRPB2	0.553	<0.001	Positive
CARD8-AS1	SIRPG	0.536	<0.001	Positive
CARD8-AS1	SIRPA	0.552	<0.001	Positive
CARD8-AS1	RASSF2	0.545	<0.001	Positive
TMPO-AS1	PCNA	0.556	<0.001	Positive
TMPO-AS1	MCM8	0.559	<0.001	Positive
TMPO-AS1	GINS1	0.594	<0.001	Positive
TMPO-AS1	TPX2	0.655	<0.001	Positive
CARD8-AS1	HCK	0.647	<0.001	Positive
TMPO-AS1	E2F1	0.619	<0.001	Positive
CARD8-AS1	SLA2	0.507	<0.001	Positive
TMPO-AS1	DSN1	0.540	<0.001	Positive
CARD8-AS1	SAMHD1	0.587	<0.001	Positive
TMPO-AS1	FAM83D	0.564	<0.001	Positive
CARD8-AS1	MAFB	0.527	<0.001	Positive
TMPO-AS1	MYBL2	0.620	<0.001	Positive
TMPO-AS1	UBE2C	0.536	<0.001	Positive
CARD8-AS1	CD40	0.545	<0.001	Positive
TMPO-AS1	AURKA	0.623	<0.001	Positive
CARD8-AS1	CASS4	0.518	<0.001	Positive
CARD8-AS1	SAMSN1	0.704	<0.001	Positive
TMPO-AS1	MIS18A	0.598	<0.001	Positive
TMPO-AS1	DONSON	0.557	<0.001	Positive
TMPO-AS1	CHAF1B	0.604	<0.001	Positive
CARD8-AS1	UBASH3A	0.527	<0.001	Positive
CARD8-AS1	ITGB2	0.534	<0.001	Positive
TMPO-AS1	CDC45	0.632	<0.001	Positive
TMPO-AS1	RANBP1	0.522	<0.001	Positive
CARD8-AS1	CRYBB1	0.588	<0.001	Positive
TMPO-AS1	MCM5	0.505	<0.001	Positive

Table S4 *(continued)*

https://dx.doi.org/10.21037/tlcr-22-500

Table S4 *(continued)*

CuRLs	mRNA	Correlation coefficient	P value	Regulation
CARD8-AS1	APOL3	0.506	<0.001	Positive
CARD8-AS1	APOL4	0.539	<0.001	Positive
CARD8-AS1	NCF4	0.645	<0.001	Positive
CARD8-AS1	CSF2RB	0.658	<0.001	Positive
CARD8-AS1	RAC2	0.556	<0.001	Positive
CARD8-AS1	CYTH4	0.670	<0.001	Positive
CARD8-AS1	MFNG	0.567	<0.001	Positive
CARD8-AS1	APOBEC3G	0.646	<0.001	Positive
CARD8-AS1	GRAP2	0.519	<0.001	Positive
CARD8-AS1	MEI1	0.513	<0.001	Positive
TMPO-AS1	CENPM	0.600	<0.001	Positive
ZSCAN16-AS1	SMDT1	0.564	<0.001	Positive
CARD8-AS1	NFAM1	0.554	<0.001	Positive
CARD8-AS1	PARVG	0.581	<0.001	Positive
TMPO-AS1	GTSE1	0.688	<0.001	Positive
CARD8-AS1	CSF2RA	0.512	<0.001	Positive
CARD8-AS1	TLR7	0.650	<0.001	Positive
CARD8-AS1	TLR8	0.693	<0.001	Positive
TMPO-AS1	FANCB	0.565	<0.001	Positive
CARD8-AS1	AP1S2	0.643	<0.001	Positive
TMPO-AS1	SCML2	0.519	<0.001	Positive
CARD8-AS1	CXorf21	0.690	<0.001	Positive
CARD8-AS1	CYBB	0.668	<0.001	Positive
CARD8-AS1	GPR34	0.706	<0.001	Positive
CARD8-AS1	GPR82	0.576	<0.001	Positive
CARD8-AS1	WAS	0.597	<0.001	Positive
TMPO-AS1	SUV39H1	0.566	<0.001	Positive
CARD8-AS1	VSIG4	0.620	<0.001	Positive
TMPO-AS1	KIF4A	0.640	<0.001	Positive
CARD8-AS1	IL2RG	0.553	<0.001	Positive
TMPO-AS1	ERCC6L	0.596	<0.001	Positive
CARD8-AS1	CYSLTR1	0.511	<0.001	Positive
CARD8-AS1	P2RY10	0.669	<0.001	Positive
CARD8-AS1	GPR174	0.598	<0.001	Positive
CARD8-AS1	ITM2A	0.553	<0.001	Positive
CARD8-AS1	SH3BGRL	0.519	<0.001	Positive
TMPO-AS1	CENPI	0.607	<0.001	Positive
CARD8-AS1	BTK	0.762	<0.001	Positive
CARD8-AS1	DOCK11	0.523	<0.001	Positive
ZSCAN16-AS1	NDUFA1	0.518	<0.001	Positive
CARD8-AS1	SH2D1A	0.695	<0.001	Positive
CARD8-AS1	SASH3	0.735	<0.001	Positive
CARD8-AS1	RAB33A	0.648	<0.001	Positive
CARD8-AS1	CD40LG	0.524	<0.001	Positive
CARD8-AS1	ARHGEF6	0.653	<0.001	Positive
CARD8-AS1	GAB3	0.585	<0.001	Positive
CARD8-AS1	MPP1	0.512	<0.001	Positive

CuRLs, cuproptosis-related lncRNAs.

https://dx.doi.org/10.21037/tlcr-22-500

Table S5 Comparisons of infiltrated immune cells between low-risk and high-risk groups

Algorithms	Immune cells	P value
TIMER	B cell_TIMER	<0.001
	T cell CD4+_TIMER	0.032
	T cell CD8+_TIMER	0.029
CIBERSORT	B cell memory_CIBERSORT	<0.001
	B cell plasma_CIBERSORT	0.042
	T cell CD4+ memory resting_CIBERSORT	0.001
	T cell CD4+ memory activated_CIBERSORT	0.02
	T cell gamma delta_CIBERSORT	0.031
	NK cell resting_CIBERSORT	0.017
	Macrophage M0_CIBERSORT	<0.001
	Macrophage M1_CIBERSORT	0.021
	Myeloid dendritic cell resting_CIBERSORT	<0.001
	Mast cell activated_CIBERSORT	<0.001
	Mast cell resting_CIBERSORT	0.001
	Neutrophil_CIBERSORT	0.002
QUANTISEQ	B cell_QUANTISEQ	0.003
	Macrophage M2_QUANTISEQ	<0.001
	NK cell_QUANTISEQ	<0.001
	T cell CD4+ (non-regulatory)_QUANTISEQ	<0.001
	T cell regulatory (Tregs)_QUANTISEQ	<0.001
	uncharacterized cell_QUANTISEQ	<0.001
MCPCOUNTER	T cell_MCPCOUNTER	<0.001
	B cell_MCPCOUNTER	<0.001
	Monocyte_MCPCOUNTER	0.01
	Macrophage/Monocyte_MCPCOUNTER	0.01
	Myeloid dendritic cell_MCPCOUNTER	<0.001
	Neutrophil_MCPCOUNTER	<0.001
	Endothelial cell_MCPCOUNTER	<0.001
	Cancer associated fibroblast_MCPCOUNTER	0.044
XCELL	Myeloid dendritic cell activated_XCELL	0.008
	B cell_XCELL	0.001
	T cell CD4+ naive_XCELL	0.001
	T cell CD4+ central memory_XCELL	<0.001
	T cell CD4+ effector memory_XCELL	0.004
	T cell CD8+ naive_XCELL	<0.001
	T cell CD8+_XCELL	<0.001
	T cell CD8+ central memory_XCELL	0.013
	Class-switched memory B cell_XCELL	<0.001
	Common lymphoid progenitor_XCELL	0.045
	Common myeloid progenitor_XCELL	<0.001
	Myeloid dendritic cell_XCELL	<0.001
	Eosinophil_XCELL	0.049
	Cancer associated fibroblast_XCELL	<0.001
	Granulocyte-monocyte progenitor_XCELL	<0.001
	Hematopoietic stem cell_XCELL	<0.001
	Macrophage M1_XCELL	0.018
	Macrophage M2_XCELL	<0.001
	Mast cell_XCELL	<0.001
	B cell memory_XCELL	0.036
	Monocyte_XCELL	0.008
	T cell NK_XCELL	0.001
	B cell plasma_XCELL	0.002
	T cell CD4+ Th1_XCELL	0.047
	T cell CD4+ Th2_XCELL	<0.001
	immune score_XCELL	<0.001
	stroma score_XCELL	<0.001
	microenvironment score_XCELL	<0.001

Table S5 *(continued)*

https://dx.doi.org/10.21037/tlcr-22-500

Table S5 *(continued)*

Algorithms	Immune cells	P value
EPIC	B cell_EPIC	<0.001
	Cancer associated fibroblast_EPIC	0.008
	T cell CD8+_EPIC	0.001
	Endothelial cell_EPIC	0.025

MCPCOUNTER, microenvironment cell populations-counter; TIMER, tumor immune estimation resource.

https://dx.doi.org/10.21037/tlcr-22-500